Meteoritics & Planetary Science 40, Nr 5, 721–743 (2005)
Abstract available online at http://meteoritics.org

In situ survey of graphite in unequilibrated chondrites: Morphologies, C, N, O, and H isotopic ratios

Smail MOSTEFAOUI[1*], Ernst ZINNER[2], Peter HOPPE[1], Frank J. STADERMANN[2], and Ahmed EL GORESY[1]

[1]Max-Planck-Institut für Chemie, Postfach 3060, 55020 Mainz, Germany
[2]Laboratory for Space Sciences and Physics Department, Washington University, St. Louis, Missouri 63130, USA
*Corresponding author. E-mail: smail@mnhn.fr

(Received 13 October 2003; revision accepted 20 March 2005)

Abstract–We performed in situ morphological and isotopic studies of graphite in the primitive chondrites Khohar (L3), Mezö-Madaras (L3), Inman (L3), Grady (H3), Acfer 182 (CH3), Acfer 207 (CH3), Acfer 214 (CH3), and St. Marks (EH5). Various graphite morphologies were identified, including book, veins, fibrous, fine-grained, spherulitic, and granular graphite, and cliftonite. SIMS measurements of H, C, N, and O isotopic compositions of the graphites revealed large variations in the isotopic ratios of these four elements. The $\delta^{15}N$ and $\delta^{13}C$ values show significant variations among the different graphite types without displaying any strict correlation between the isotopic composition and morphology. In the Khohar vein graphites, large ^{15}N excesses are found, with $\delta^{15}N_{max}$ ~+955‰, confirming previous results. Excesses in ^{15}N are also detected in fine-grained graphites in chondrites of the CH clan, Acfer 182, Acfer 207, and Acfer 214, with $\delta^{15}N$ ranging up to +440‰. The ^{15}N excesses are attributed to ion-molecule reactions at low temperatures in the interstellar molecular cloud (IMC) from which the solar system formed, though the largest excesses seem to be incompatible with the results of some recent calculation. Significant variations in the carbon isotopic ratios are detected between graphite from different chondrite groups, with a tendency for a systematic increase in $\delta^{13}C$ from ordinary to enstatite to carbonaceous chondrites. These variations are interpreted as being due to small- and large-scale carbon isotopic variations in the solar nebula.

INTRODUCTION

Carbon is one of the most abundant and widely distributed elements in nature, and one of the most versatile elements in terms of the number of compounds it may form. In meteorites, the presence of various chemical forms of carbon (e.g., organic compounds, carbonates, carbides, diamond, graphite, etc.) represents one of the best sources of information about the origin and evolution of carbonaceous matter in the early solar system. In chondrites, which preserve the most primitive meteoritic matter (i.e., are least modified by secondary events such as planetary differentiation), most of the carbon is present in organic and elemental form. Although many studies have been conducted to investigate the amount, distribution, and isotopic compositions of carbonaceous matter, the origin and evolution of most of the carbon components are still controversial, and only a small amount of carbon (graphite, diamond, silicon carbide) in the most primitive chondrites is known to be of interstellar origin (Anders and Zinner 1993; Huss and Lewis 1995).

Since the first descriptive studies of graphite in meteorites by Kurat (1970) and Ramdohr (1973) little attention was devoted to the study of elemental carbon in primitive chondrites. Only recently, several studies revealed pristine records of early solar system events to be preserved in carbon (Brearley 1999; Mostefaoui et al. 2000; Sugiura and Kiyota 1998; Sugiura and Zashu 2001). These studies showed that graphite is a very common phase in the most primitive chondrites and is mostly associated with Fe-Ni metal (called metal-associated carbon or MAC by Mostefaoui et al. [2000]). The presence of large isotopic heterogeneities of C and N in graphite from the differentiated Acapulco meteorite (El Goresy et al. 1995) revealed that graphite is a highly retentive phase for isotopic signatures which survived extended heating to solidus temperatures of up to ≈1200 °C (Zipfel et al. 1995). Since unequilibrated chondrites are much less heated than Acapulco, their graphite is expected to even better preserve pristine records, and thus to play the role of a tracer of conditions in the early solar nebula.

In this paper, we report detailed in situ microscopic

studies of morphologies, textures, and assemblages of graphite in ordinary, enstatite, and carbonaceous chondrites. We also report in situ isotopic measurements of carbon and of the trace elements hydrogen, nitrogen, and oxygen in graphite that were performed in order to search for correlations between morphologies and isotopic compositions, to characterize graphite of solar system origin in comparison to interstellar (presolar) graphite, and to search for assemblages containing graphite originating outside the solar system.

EXPERIMENTAL PROCEDURES

Samples

Ten polished sections from four ordinary chondrites, three carbonaceous chondrites, and one enstatite chondrite were carefully prepared and searched for the occurrence of graphite. The chondrites are Khohar, Mezö-Madaras, Inman (L3), Grady (H3), Acfer 182, Acfer 207, Acfer 214 (CH3), and St. Marks (EH5). Table 1 shows some of the properties of these chondrites and the sizes of the investigated polished sections.

Optical microscopy in reflected light was extensively used during this study in order to identify graphites in the samples and to recognize their morphologies between crossed nichols (El Goresy 1965). Large graphites are easily identified and classified in the optical microscope. Smaller ones (i.e., <1 μm) are more easily detected in the scanning electron microscope (SEM). A Cambridge 180 SEM at the MPI für Kernphysik in Heidelberg, Germany was used for that purpose. Because the morphology of graphite cannot be determined in the SEM, grains <1 μm could not be classified. Their morphologies thus remain unknown, and we will refer to them as fine-grained graphite.

SIMS Measurements

Isotopic ratios of hydrogen, carbon, nitrogen, and oxygen in the graphites were measured with the ion microprobe. Two Cameca IMS 3f ion microprobes (one at Washington University in St. Louis, USA, the other at the University of Bern, Switzerland) were used for the carbon, hydrogen, and nitrogen isotopic measurements. Isotopic analyses were made on sample areas of about 2–3 μm in diameter, with a primary beam of Cs^+ ions. Carbon and N were measured together, using negative secondary ions of C and CN, following the procedure described by Zinner et al. (1989). In order to minimize surface contamination, the analysis spots were pre-sputtered for before each measurement. Because the analysis of C and N and the analysis of H require different settings of the ion microprobe instruments, the H isotopes were measured independently from the C and N isotopes. In most cases negative secondary ions of H were measured alone, but in eight graphite grains in Khohar, we also included C^- and CN^- in the measurements in order to simultaneously determine the N and H contents of these grains. For the C and N isotopic analyses the mass resolving power of $m/\Delta m \approx 6000$ was sufficient to separate ^{13}C from ^{12}CH, $^{12}C^{15}N$ from $^{13}C^{14}N$, and $^{12}C^{14}N$ from $^{12}C^{13}CH$. Contributions from $^{13}C_2$ to $^{12}C^{14}N$, which are not fully separated under these conditions, can generally be neglected. For H isotopes, isobaric interferences are negligible at low mass resolving power (McKeegan et al. 1995). Analyses of meteoritic graphites were alternated with measurements of a laboratory carbon and nitrogen standard (DAG) with known isotopic compositions, which had been deposited on the periphery of the sample mount. The H isotopic data are normalized to SMOW with the help of a terrestrial standard "the Washington University amphibole standard" because previous studies have shown that H isotopic analysis with negative secondary ions is much less subjected to matrix effects than analysis with positive secondary ions. Nitrogen and H concentrations (see Tables 3 and 4) were calculated from the H^-/C^- and CN^-/C^- ratios using the relative sensitivity factors published by Hoppe et al. (1995). These factors are 0.3×10^6 and 0.07×10^6 for H and N, respectively, if the resulting H and N concentrations are expressed in ppm weight. Since large matrix effects were observed by Hoppe et al. (1995), the estimated concentrations lower than 2 wt% are considered accurate only within a factor of 2–3. For higher concentrations, the obtained values are overestimated (see Huss et al. 1997). Accordingly, N concentrations higher than 2 wt% in Table A1 need to be considered as upper limits.

Isotopic measurements of oxygen in graphites were conducted for Khohar and Mezö-Madaras with the Washington University ion microprobe. We used a primary beam of Cs^+ ions and a mass resolving power of ≈5600 in order to resolve $^{17}O^-$ from $^{16}OH^-$. Laboratory graphite was used as a standard. Since many of the meteoritic graphites are fine-grained and mixed with Fe-Ni metal, and in most cases had been extensively sputtered during previous measurements, contamination from the surrounding phases probably contributed to the analyses. The oxygen isotopic results should thus be considered with caution.

PETROGRAPHY OF GRAPHITE

Graphite shows significant variations among the investigated chondrites concerning its mode of occurrence, abundance, association with other mineral phases, and morphology.

Texture and Assemblages

In the investigated chondrites, graphite is found in all textural units, i.e., chondrules, matrix, and chondrule rims. Figure 1 shows low magnification optical microscope images of polished sections from Khohar, Mezö-Madaras, and Grady, which are the three most graphite-rich chondrites in this study. The rectangles in Fig. 1 indicate the areas where

Table 1. Chondrites selected for the search of graphite.

Chondrite	Type	Sections	S (cm^2)	Brecciation	[C][a] (ppm)	Bulk $\delta^{13}C$ (‰)
Khohar	L3	2	1.64	Yes	3650[b]	–20.7[b]
Mezö-Madaras	L3	2	1.70	Yes	1930[b]	–23[b]
Inman	L3	1	0.86	No	3900[c]	–19.6[c]
Grady (1937)	H3	1	0.88	Yes	3100[d]	–25.6[d]
Acfer 182	CH3	1	3.20	No	3500[e]	0.3[e]
Acfer 207	CH3	1	0.39	No	3500[f]	0.3[f]
Acfer 214	CH3	1	3.85	No	3500[f]	0.3[f]
St. Marks	EH5	1	0.4	No	5320[g]	–10.7[g]

[a][C] total carbon concentrations in the chondrites of this study.
[b] Grady et al. (1989)
[c]Since no data are available in the literature about bulk C in Inman determined by stepped combustion, we adopted a value for bulk C calculated from the Inman carbon content of an insoluble residue by Alexander et al. (1998),the carbon fraction in Inman given by Morse et al. (1989), and from a bulk value for $\delta^{13}C$ for the mean of type 3 ordinary chondrites determined by Grady et al. (1989).
[d]Grady et al. (1982)
[e]Grady et al. (1991)
[f]Grady et al. (1986)
[g]Same values as for the paired chondrite Acfer 182.

graphites are found. In Khohar and Mezö-Madaras, the graphites are almost uniformly distributed throughout the sections, with the highest concentrations in the matrix and in chondrule rims.

Graphite in Grady is mostly concentrated in a metal-poor region consisting of dark silicate grains that, according to SEM BSE images, are chemically distinct from the main chondrite host. Although the boundaries are not so sharply delineated, its texture and distinct chemical composition strongly suggest that it is a portion of a clast. A more quantitative investigation is, of course, needed, but this is beyond the scope of this paper at the moment. In St. Marks (see also El Goresy et al. 1988), graphite is present in all textural units except in chondrules, and it has no preference for a particular petrographic context. In Inman, Acfer 182, Acfer 207, and Acfer 214, graphite is rare.

Graphite in the investigated chondrites is usually associated with Fe-Ni metal (Fig. 2). This graphite was defined as MAC by Mostefaoui et al. (2000). In Khohar, a large amount of graphite is found in a metal-rich chondrule rim (Fig. 3); we estimate the carbon to represent at least 30% of the rim. This is the highest concentration of carbon ever reported in a chondrule rim. In our samples, in addition to MAC, we found assemblages consisting of large amounts of graphite associated either with silicate, troilite, or Fe oxide (Fig. 2). Some of these phases also contain metal, but since the most dominant phases associated with the carbon are silicate, troilite, or Fe oxide, we named these occurrences of graphite silicate-, troilite-, and oxide-associated carbon (hereafter SAC, TAC, and OAC). The idea behind this classification is to determine to what extent the graphite can be genetically related to its surrounding phases. For instance, the MAC surrounding the chondrule in Fig. 3 is also in contact with the chondrule silicates and with the silicates outside the chondrule. However, since the petrography clearly shows that the carbon is related to the metal (e.g., it occurs as a complex mixture between the two phases), we classified it as MAC. The same applies for the other associations. Since we only have access to two-dimentional sections of meteoritic samples, graphite that apparently is touching a phase could very well be associated with other phases in the third dimension. As a result, we cannot totally exclude the possibility that some associations are incorrectly classified.

Abundance

Although graphite is common in chondrites, its presence in assemblages having wide size ranges and its possible distribution all over the polished sections make a precise estimate of its abundance quite a challenging task. Mostefaoui et al. (2000) used a method based on the number of metal grains in the samples and the proportion of graphite-bearing metal in order to obtain quantitative estimates of the abundance of graphite-bearing metal and thus a measure of the MAC abundance in chondrites. While this method determines the abundance of the graphite-bearing metal, even though it does not necessarily provide the graphite abundance, it cannot be applied here because MAC is not the only (or even major) graphite type in our samples. Hence, the abundance of the graphite can only be qualitatively estimated. More quantitative conclusions, in fact, can be made about the relative proportions of the various graphite-bearing assemblages within the same chondrite. Because of the small differences in the size distributions among the different graphite associations, we assume that there will be no bias in the relative proportions.

In order to estimate the relative proportions of MAC, SAC, TAC, and OAC, we counted the number of graphite-bearing assemblages in each of our chondrite sections under the optical microscope. The proportions of the graphite-bearing assemblages are expected to vary considerably as a function of the lower optically resolvable size limit in the search. Here, we only considered graphite assemblages

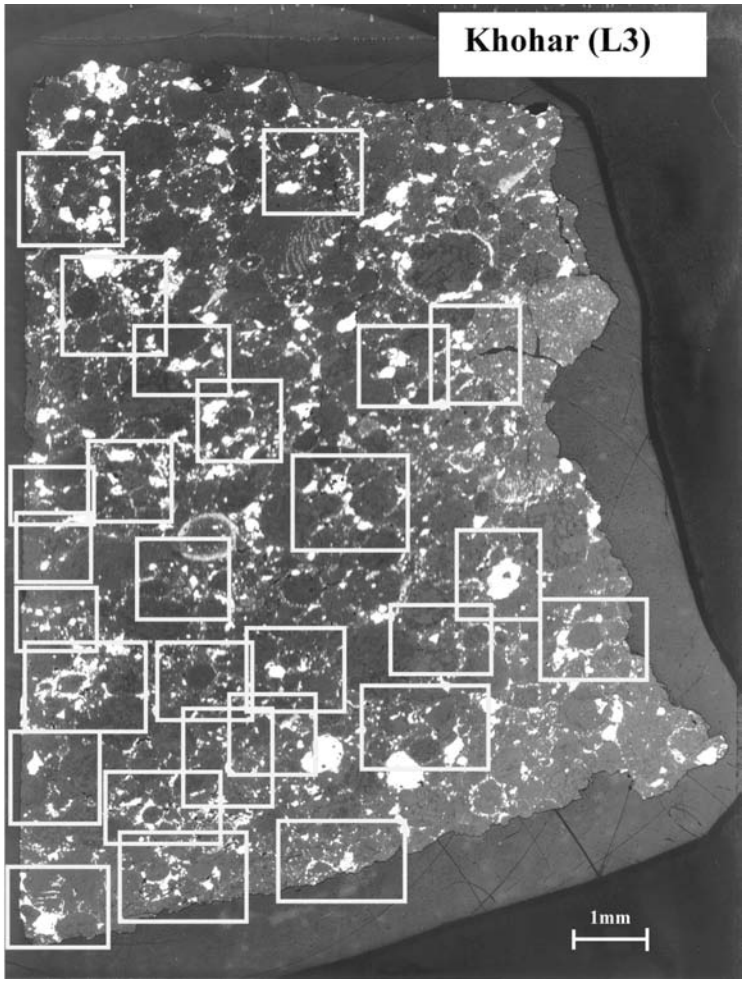

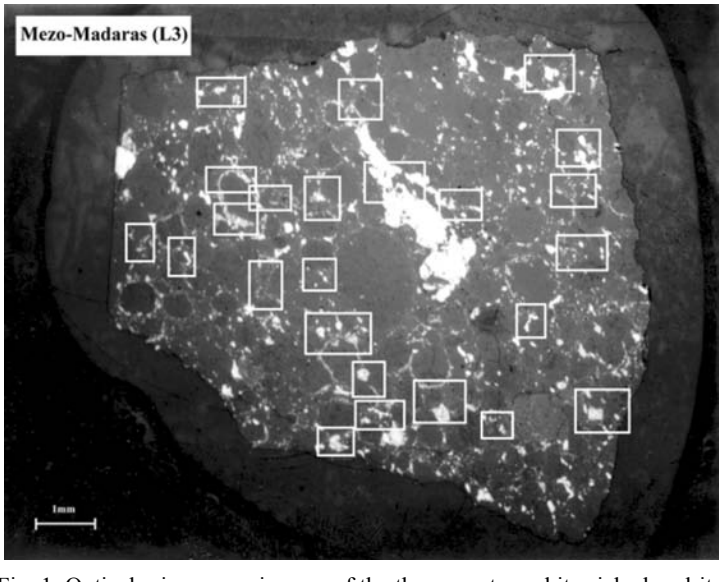

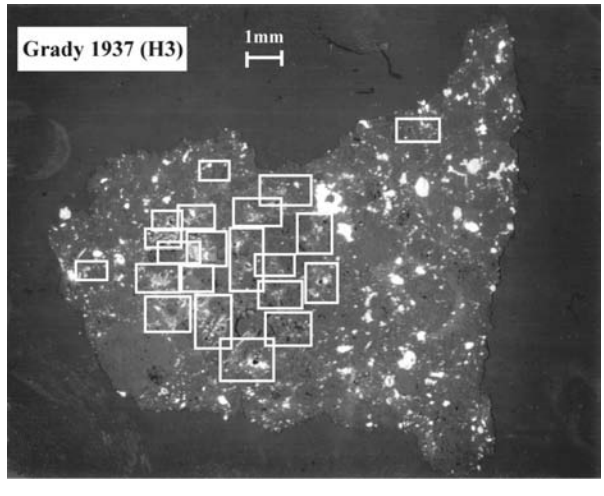

Fig. 1. Optical microscope images of the three most graphite-rich chondrite sections studied here (Khohar, Mezö-Madaras, and Grady). The rectangles depict areas where graphite is found. In Khohar and Mezö-Madaras, the graphites are almost randomly distributed, while in Grady most of the carbon is concentrated in a metal-poor region.

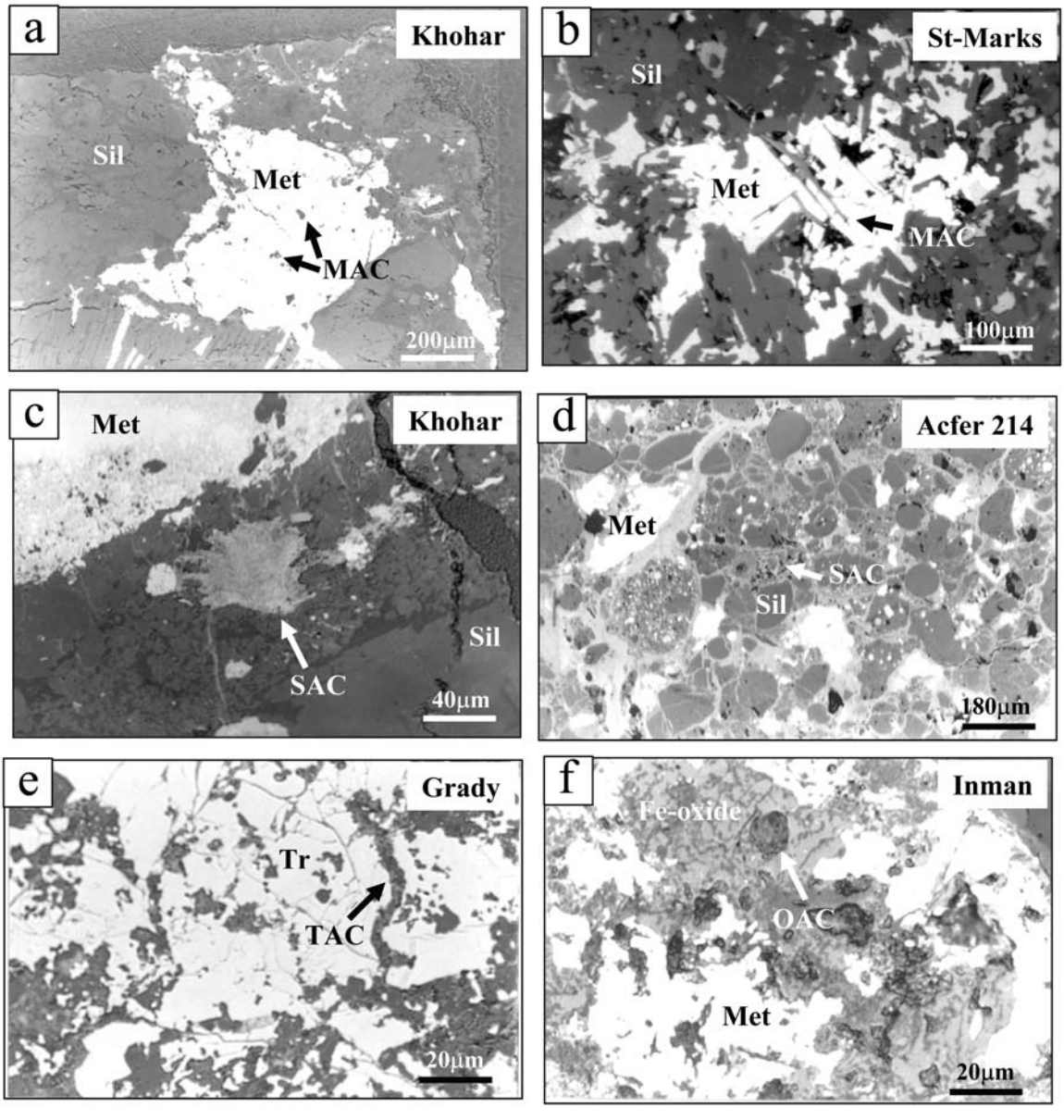

Fig. 2. Optical microscope images showing different occurrences of graphite in chondrites. a) A metal-associated carbon (MAC) in Khohar consisting of graphite inclusions of several micrometers in sizes. b) Elongated graphite books in metal in the St. Marks chondrite. c) A silicate-associated carbon (SAC) consisting of a mixture of fiber and book graphite in Khohar. d) SAC in Acfer 214 consisting of a mixture of fine-grained and book graphite (see Figs. 4c and 4d for higher magnification images). e) Troilite-associated carbon (TAC) in Grady. A long curved chain composed of graphite books is visible near the center of the picture. f) An oxide-associated carbon (OAC) in Inman consisting of a granular graphite grain entirely surrounded by Fe oxide. The presence of metal enclaves suggests that the Fe oxide was formed by alteration of the Fe-Ni.

having sizes >~5 μm. We believe this to be a reasonable limit, at least as a first approximation, since because of their scarcity (judged from optical microscopic observation) we do not expect smaller graphite assemblages to contribute significantly to the total graphite abundance in the meteorite.

The relative proportions of MAC, SAC, TAC, and OAC are given in Table 2. In Khohar and Mezö-Madaras, most of the carbon is present as MAC and SAC. In Inman, MAC is the most abundant type. In Grady, a large proportion of the graphite is found in troilite, and MAC represents only ~5%. In the paired Acfer chondrites, MAC is clearly lower than SAC, and in Acfer 214, MAC was not encountered. In Acfer 207, more than 40% of the graphite is associated with Fe oxide and is distinct from that in Acfer 182 and Acfer 214. In St. Marks, MAC is the dominant graphite type (see also El Goresy et al. 1988) but a fairly large proportion of TAC is also present.

Using the counted numbers of the graphite-bearing assemblages and taking into account the explored sample

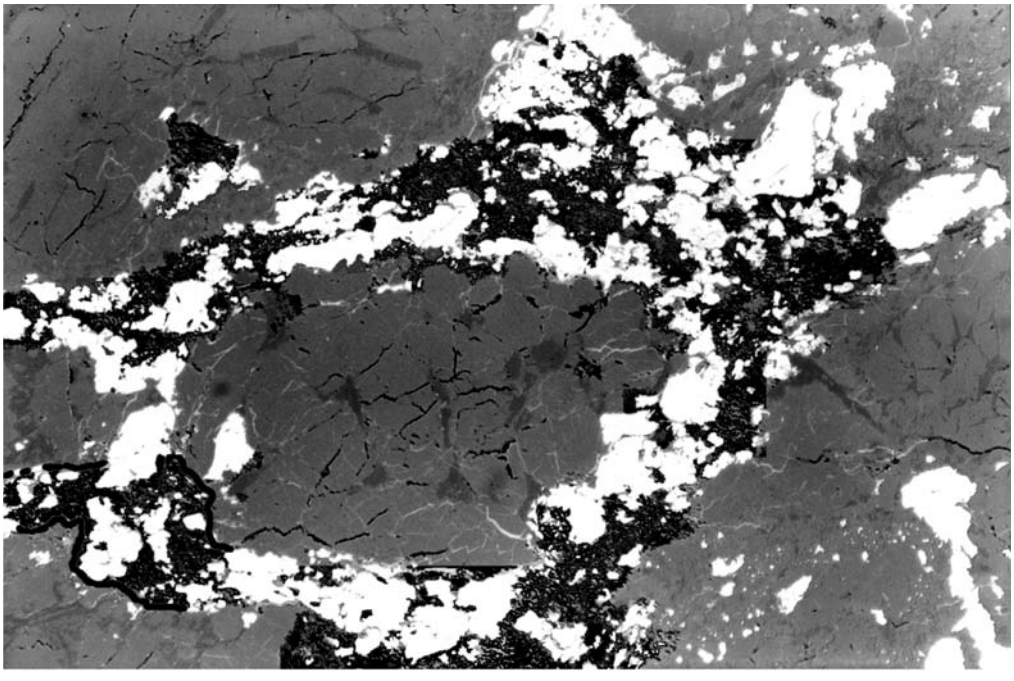

Fig. 3. A metal-rich chondrule rim in Khohar containing a large amount of graphite (black). The carbon represents more than 30% of the rim.

Table 2. Graphite morphologies and their associated minerals in chondrites.

Chondrite	Graphite	Proportion (%)				Morphology[a]
		MAC	SAC	TAC	OAC	
Khohar	Abundant	42	47	10	1	B>Fb>>V>S>G~F
Mezö-Madaras	Abundant	46	38	16	0	B>Fb>>V>S>G
Inman	Rare	69	6	0	25	B>Fg>G~C
Grady (1937)	Abundant	5	43	41	11	B>Fg>>Fb>G~C
Acfer 182	Rare	10	62	0	28	B>Fg
Acfer 207	Rare	15	43	0	42	B>Fg
Acfer 214	Rare	0	85	0	15	B>Fg
St. Marks	Abundant	42	25	33	0	B

MAC, SAC, TAC and OAC are respectively metal-, silicate-, troilite-, and oxide-associated carbon.

[a]B: books, Fg: fine-grained, S: spherulitic, Fb: fibers, G: granular, C: cliftonite, F: feathery. The > symbol indicates the order of abundance of a given morphology in the chondrite.

areas under the optical microscope, one can qualitatively determine that Khohar is the meteorite most enriched in graphite, followed by Mezö-Madaras, Grady, and then St. Marks. The Acfer 207 and Inman chondrites have intermediate abundances, while Acfer 214 and Acfer 182 show low graphite abundances.

Morphologies

Various graphite morphologies are encountered in the investigated chondrites, with grain sizes ranging from <0.5 to ~15 μm. Reflected light optical microscope images of different graphite morphologies are shown in Figs. 4 and 5. Their relative abundances in the chondrites are indicated in Table 2.

The morphologies encountered in the studied chondrites include books (B), spherulitic (S), granular (G), cliftonite (C), single fibers (Fb), veins (V), polycrystalline fine-grained aggregates (Fg), and feathery (F) graphite. Books are the most abundant graphite type. Their single crystals of stacked open sheets make them easily recognizable between crossed Nichols through high birefringence. The books usually form aggregates with silicate, metal, and around troilite grains (Figs. 4a–b). Their sizes generally do not exceed a few microns, but single crystals of more than 10 μm in length are found in St. Marks (Fig. 2b). Fine-grained graphite is the second-most abundant type. It does not exceed ~0.5 μm in size and it usually fills the spaces between graphite books. The small grain size of this type did not allow us to identify its morphology under the optical microscope. Fine-grained graphite and books are generally associated with each other and form large graphite mixtures, reaching several hundreds of microns in the Acfer clan chondrites (Fig. 4c–d). The graphite fibers are rolled-up graphite sheets. They are

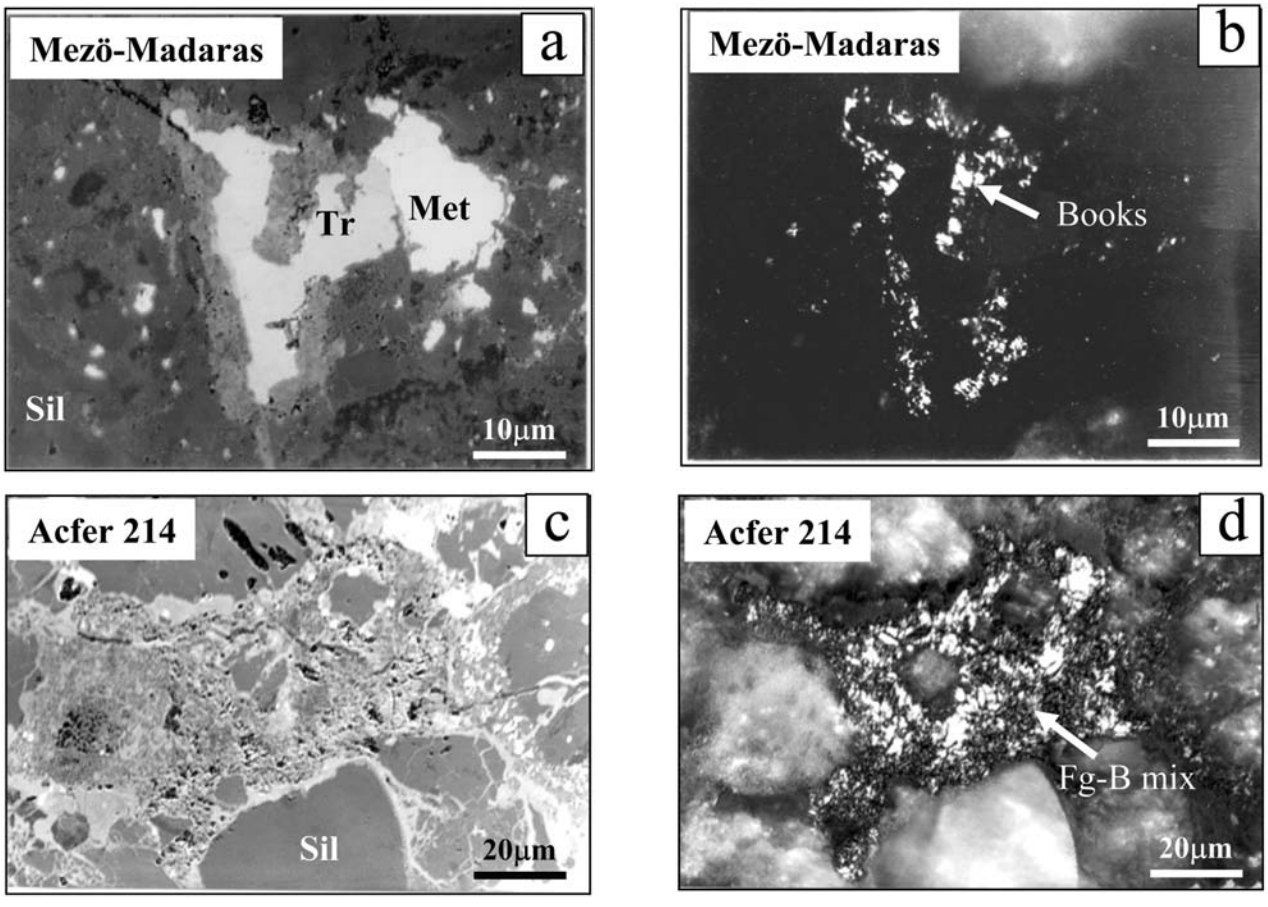

Fig. 4. Optical microscope images showing the morphology of graphite in chondrites. a) A troilite grain in Mezö-Madaras is surrounded by single graphite books. b) An image of the same area in Mezö-Madaras under crossed nichols. The orientations of the open sheets of the graphite books around the troilite are visible. c) The SAC fine-grained book mixtures in Acfer 214 shown in Fig. 2d. d) An image of the same area in Acfer 214 under crossed nichols. The large bright areas are graphite books while the tiny ones are fine-grained graphite.

commonly observed in Khohar and Mezö-Madaras, parallel to each other (Fig. 5b) and in some cases jointly growing with the books and the fine-grained graphite. In contrast to these types, the spherulitic, cliftonite, feathery, and granular graphites are always found as individual grains in metal; they are up to 15 μm in size (Figs. 5c, d, e). Spherulitic graphite is less common in Khohar and Mezö-Madaras than in Bishunpur (Mostefaoui et al. 2000). In Mezö-Madaras we found another occurrence of a spherulitic graphite grain in troilite (Fig. 5e), in addition to the finding in the Kainsaz carbonaceous chondrite (Mostefaoui et al. 2000). Granular graphite is rare and only exists in metal (Fig. 5c) and in Fe oxide (Fig. 2f). In Khohar, different graphite types can be found in a single metal grain (Fig. 5c). Among them are several feathery graphites representing the first occurrence of this type in a chondrite (Fig. 5c). Graphite veins are present only in Khohar and Mezö-Madaras (Fig. 5a). They are mostly associated with shocked metal-troilite assemblages and are known to have large N isotopic anomalies (Mostefaoui et al. 2000).

ISOTOPIC COMPOSITIONS

Carbon and Nitrogen

Carbon and nitrogen isotopic ratios measured in graphite are listed in Table A1 in the appendix, and in Fig. 6. They are given as δ values, deviations from the standard isotopic ratios (Pee Dee Belemnite (PDB) for $^{13}C/^{12}C$; Air for $^{15}N/^{14}N$) in permil. Hashizume et al (2000) proposed a solar N isotopic composition 24% lighter than the terrestrial atmosphere, which would mean that the ^{15}N enrichments in our samples relative to the solar composition may be considerably higher than the values noted here. The carbon isotopic ratios are all close to normal (i.e., within the range found in terrestrial samples; In this paper we refer to the terrestrial isotopic ratios as normal) and most $\delta^{13}C$ values are negative. However, among the chondrites there is a large scatter with $\delta^{13}C$ values ranging from −53‰ in Khohar to 40‰ in Acfer 182. Smaller but significant variations are detected in graphites within a given chondrite. In Khohar, for

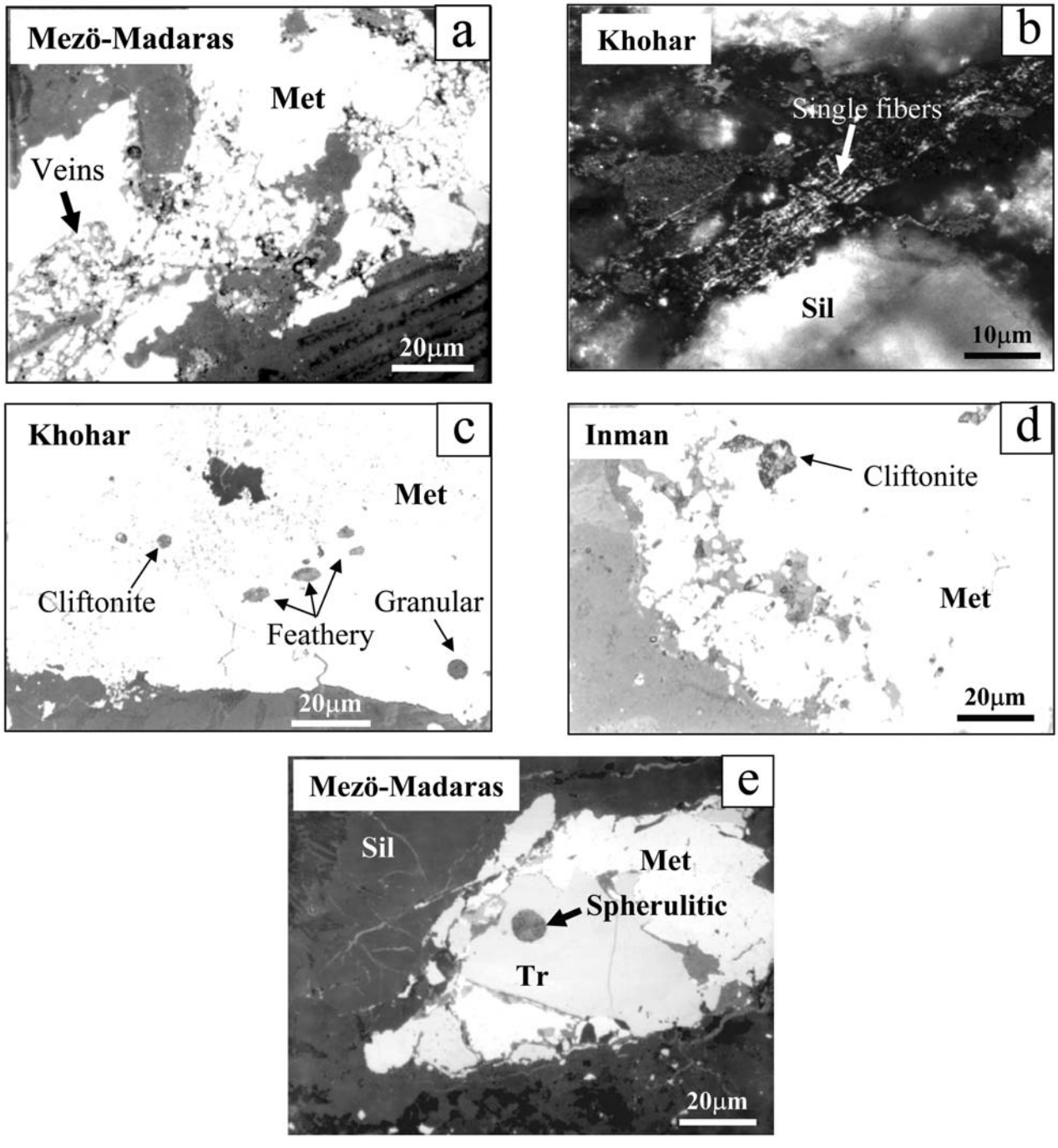

Fig. 5. Optical microscope images showing the morphology of graphite in chondrites. a) Large metal grains in Mezö-Madaras containing high concentrations of very thin graphite veins. Note that some parts of the metal are free of graphite veins. b) Image of SAC in the matrix of Khohar under crossed nichols. The graphite is composed of single fibers aligned parallel to each other. c) A metal grain in Khohar contains graphite inclusions of cliftonite and blebs with granular and feathery morphologies. d) This image, taken between partially crossed nichols, shows a cliftonite inclusion in a metal grain from Inman. The cubic morphology of the cliftonite is recognized from the orientation of its graphite books. e) A spherulitic graphite inclusion in a Mezö-Madaras troilite grain. The morphology is apparently generated by graphite needles growing from the center of the inclusion.

example, $\delta^{13}C$ ranges from −14 to −53‰, a variation of about 40‰. In this chondrite, variations up to 10‰ exist in graphite within single metal grains (e.g. 1AR1-1 to 1AR1-11 in Table A1). While most graphites have negative $\delta^{13}C$ values, a few of the analyzed graphites in Acfer 182 and more than the half in St. Marks have positive values.

The nitrogen isotopic ratios in graphite show a much larger scatter among the chondrites than those of carbon, and

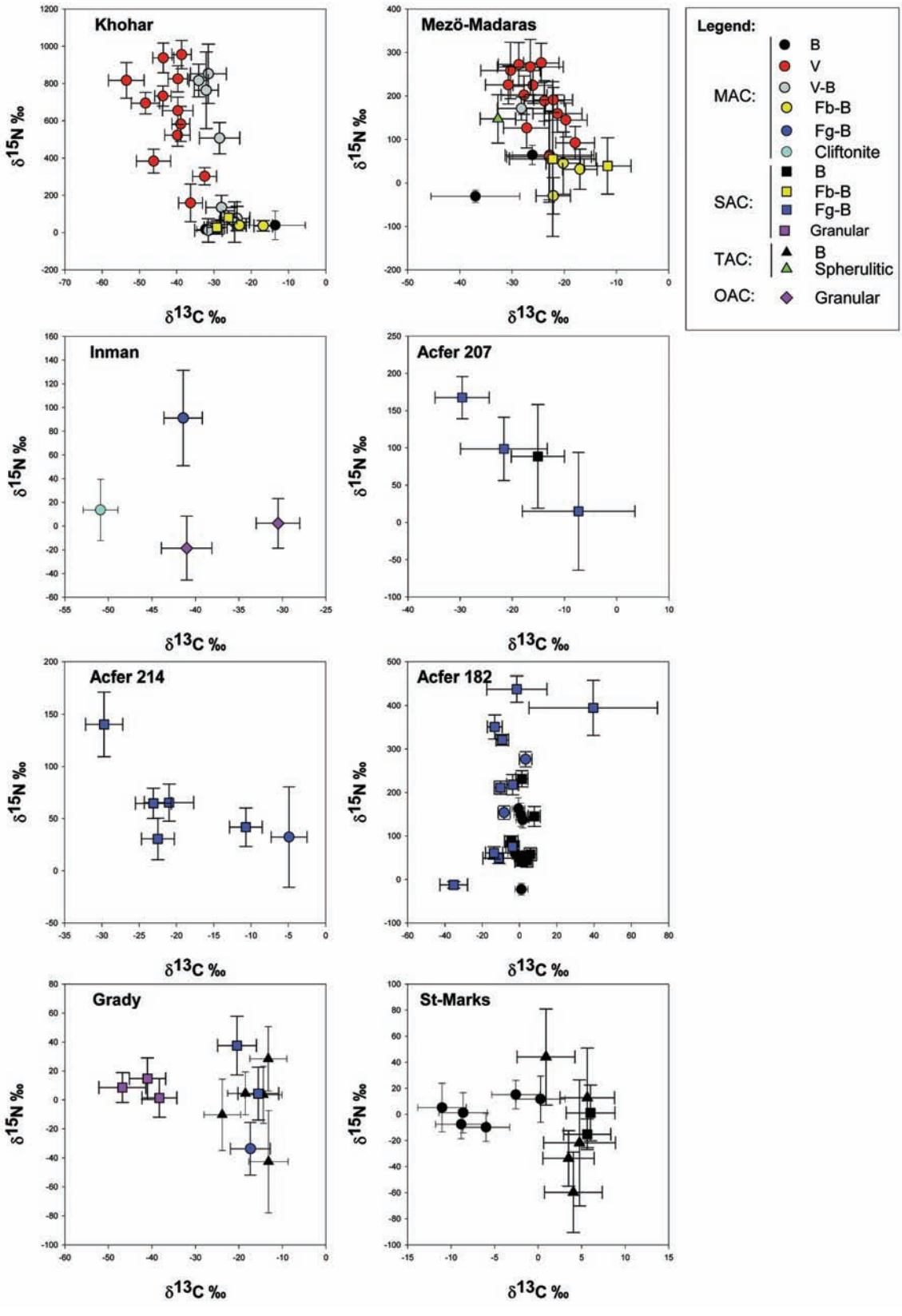

Fig. 6. Plots of $\delta^{15}N$ versus $\delta^{13}C$ measured in graphite with various morphologies from eight chondrites. Different symbols and different colors represent different occurrences and different morphologies, respectively (legend: B = books; V = vein; Fb = fibers; Fg = fine-grained). Errors are 1σ.

$\delta^{15}N$ values are positive in most of the measured graphites. While Inman, Grady, and St. Marks exhibit close-to-normal N isotopic ratios, large ^{15}N excesses are found in Khohar, Mezö-Madaras, Acfer 182, Acfer 207, and Acfer 214 (Fig. 6). In Khohar, $\delta^{15}N$ values reach 955‰. This confirms the large ^{15}N enrichments (up to 1135‰) previously obtained in graphite of this chondrite (Mostefaoui et al. 1998). The maximum $\delta^{15}N$ value in Acfer 182 is 438‰ (Fig. 6). Graphite in Acfer 182 is possibly related to the carrier of heavy N found in the bulk acid-resistant residues from the same meteorite by Grady and Pillinger (1993), although the ^{15}N excesses found in the present study fall short of those measured in the residues (up to 1584‰).

Figure 6 shows correlation plots between the N and the C isotopic ratios for graphites of different texture and morphology. There appears to be a negative correlation between $\delta^{15}N$ and $\delta^{13}C$ in Khohar, Mezö-Madaras, and Acfer 207 with heavy N being encountered in graphites with low $\delta^{13}C$ ratios. The highest $\delta^{15}N$ values in Khohar and Mezö-Madaras (up to 955‰ and 272‰, respectively) were found in graphite veins and in vein-book graphite mixtures in MAC (e.g., Fig. 5a). The fact that N in individual graphite books is isotopically normal (see Fig. 6 and Table A1 in the appendix) suggests that vein graphite is the sole carrier of the N anomaly in these chondrites. In Mezö-Madaras, a TAC spherulitic graphite grain has a ^{15}N excess of ~150‰ (Fig. 5e). This is the highest excess reported in a spherulitic graphite grain. In the Acfer chondrite clan, the largest ^{15}N excesses are found in fine-grained books mixtures ($\delta^{15}N_{max}$ ~450‰). In contrast to Khohar and Mezö-Madaras, where the highest $\delta^{15}N$ values are present in MAC, in the Acfer chondrite clan they are mostly found in SAC. The small grain size of the fine-grained graphites and their close connection to the books did not allow us to measure them separately. Therefore, we do not have direct isotopic information from this type. Note that the fine-grained books mixtures show more variable C isotopic ratios than the individual books.

Except for St. Marks and Grady there is no obvious correlation between graphite texture and morphology and the C isotopic signatures. In St. Marks, although the graphites are all books, MAC seems to have lower $\delta^{13}C$ and higher N concentrations than graphite of the other textures (Table A1). More interestingly, in Grady, two groups with distinct $\delta^{13}C$ values can be distinguished (Fig. 6), granular SAC having low $\delta^{13}C$ of about −40 to −50‰. Also, this type has higher N contents than the other coexisting types (see Table A1).

Hydrogen

A total of 87 measurements of H isotopic ratios were made on six graphite assemblages from Khohar and five from Mezö-Madaras (Table A2). All results are normalized to SMOW. D/H measurements in Khohar were made on MAC veins and in Mezö-Madaras on MAC veins, books, and vein-books mixtures. The vein graphites in Khohar show positive δD values with a maximum of 336‰. This is lower than the 1500‰ found in graphite from the same chondrite (Mostefaoui et al. 1998), showing that the graphites have distinct H isotopic signatures. In Mezö-Madaras, most of the δD values are around −200‰. In some graphites, after sputtering for a long time we noted a clear increase in the D/H ratio. This can be interpreted as being due to the removal of contaminated layers. In order to determine the variation of the H isotopic ratio with depth we made between 2 and 13 consecutive measurements in the same graphite areas. Figure 7 shows the profiles recorded in each measured area. An increase in δD with depth is seen in most of the analyzed graphites. The highest increase in δD with depth was observed in vein graphites, with a maximum δD of +600‰ as we sputtered into deeper graphite layers. Such increases are a clear indication of the removal of contaminated surface layers by ion sputtering. In our samples, contamination with water of normal isotopic composition during polishing was possibly responsible for lowering δD values. Sugiura and Kiyota (1998) reported that analysis of graphite in a preheated sample of Mezö-Madaras gave a δD value of about +2800‰, which is more than 4 times as high as our maximum values. Since the authors did not give any errors, nor provide any analysis conditions, these values must be considered with caution. Nevertheless, the vein graphites in our samples show a clear enrichment in D compared to the book graphites (Fig. 7), suggesting the presence of two distinct H isotopic signatures.

Oxygen

Oxygen isotopic measurements were made on 6 MAC (4 veins and 2 vein-book mixtures) in Khohar and 15 MAC veins in Mezö-Madaras (Table A3). Although the data are limited in number, the results reported here are the first in situ measurements of oxygen isotopic ratios in graphite from chondrites. Figure 8 shows the oxygen isotopic results in a δ value 3-isotope plot. All graphites have normal oxygen isotopic compositions (i.e., no extreme deviating from the terrestrial standard value). Since the data are normalized to a terrestrial graphite standard and not to SMOW, we do not really know where the terrestrial fractionation and the Allende mixing lines are in this diagram (they are only shown here for general orientation). The errors of these measurements are relatively large compared to other oxygen measurements made in St. Louis with the ims 3f ion probe. This is due to the fact that the graphite is poor in oxygen in the first place, and that small graphite particles analyzed are located adjacent to oxygen-rich phases.

No differences are seen in O isotopic compositions between the vein and the vein-book graphite mixtures, except for one measurement of only ^{16}O and ^{18}O isotopes of a vein graphite from Khohar. In this vein we found a large change in the isotopic ratio during the analysis. Figure 9 shows $\delta^{18}O$

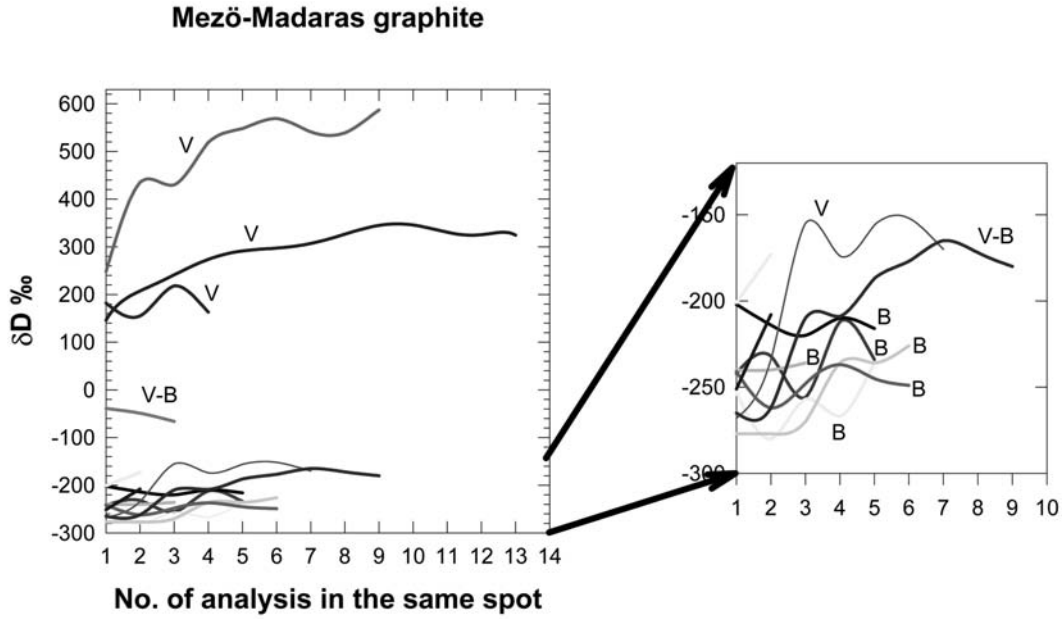

Fig. 7. Variation of δD with time (expressed as analysis number on a given sample spot) for vein and book graphites in Mezö-Madaras. The strong increase in δD with time in some cases indicates the removal of surface contamination. The vein graphites show clear enrichments in D compared to the books.

results for a 15-block analysis. Depletions in ^{18}O, with $\delta^{18}O$ as low as −100‰ in the first block, were initially detected; subsequently $\delta^{18}O$ increased gradually with time toward a normal value. This analysis hints at the presence of a small phase (probably not exceeding one micron) of isotopically anomalous material that was sputtered away during the measurement. However, since we only measured two oxygen isotopes, we cannot tell where this anomalous composition plots on an oxygen 3-isotope plot. Attempts to reproduce this result with a 3-isotope oxygen measurement at the same location were not successful.

DISCUSSION

The presence of graphite in unequilibrated chondrites raises a number of questions about its origin, the formation mechanism of its various morphologies, and the history of the isotopic compositions of its constituents. Here, we will discuss several key issues in order to help in understanding the mechanisms that formed the graphite and the conditions under which the carbonaceous precursor matter formed and evolved in the solar system.

Do the Graphites In Chondrites Have a Pre-Accretionary Origin or Are They Products of Parent Body Metamorphism?

One of the major questions that need to be addressed in detail is whether graphite in chondrites is of primary or secondary origin (meteoriticists also use the terms pre- and post-accretion in order to describe events that affected chondritic phases before or after material compaction that led to the formation of planetesimals). Solar nebula condensation, chondrule formation, thermal metamorphism, and impacts on parent bodies are all processes that significantly affected chondritic materials during early solar system evolution. Chondritic graphite has probably gone through, or was produced during, one or more of these events, which might leave some records on the carbon. Brearley (1990) has suggested that carbon-rich aggregates in chondrites are post-accretionary phases, catalytically graphitized carbonaceous matter that was produced during planetary processing at temperatures between 300 and 450 °C. Poorly graphitized carbon (PGC) in Allende has also been attributed to parent body processes, because it would have been unstable at the high temperature conditions of the solar nebula (Brearley 1999). The common association of graphite and metal in our chondrite samples could be evidence that the carbon was produced during parent-body thermal metamorphism, e.g., by exsolution of pre-existing carbon in metal or through the breakdown of carbides. The graphite lamellae in enstatite chondrites have been attributed to exolution from metal (El Goresy et al 1988). Support for this view has been provided by experiments at temperatures comparable to those typical for chondritic metamorphism, in which the transformation of carbides or carbon-containing metal to α-iron was accompanied by exsolution of elemental carbon, because α-iron cannot take up that much carbon (Brett and Higgins 1967; Romig and Goldstein 1978). However, we have several pieces of evidence that most of the chondritic graphite of this study is of primary origin, i.e., formed before accretion of the parent asteroids.

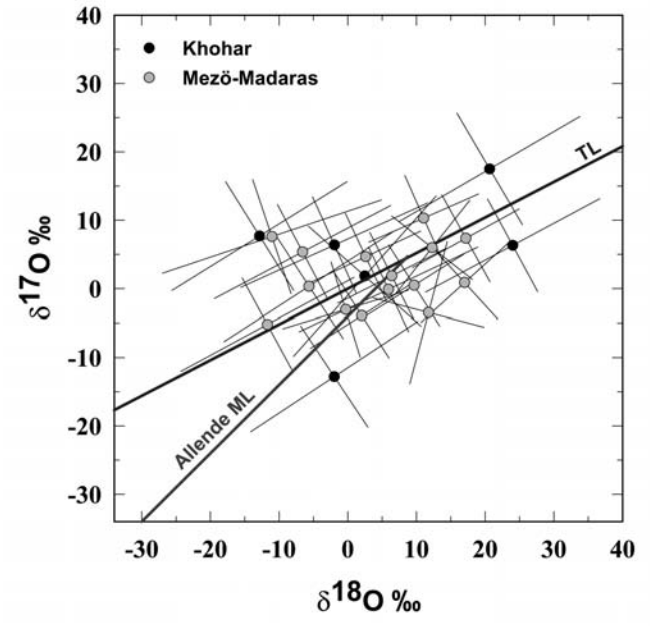

Fig. 8. Plots of $\delta^{17}O$ vs. $\delta^{18}O$ for vein graphites and vein-book graphite mixtures in Khohar and Mezö-Madaras. Allende ML: Allende mixing line. TL: terrestrial fractionation line. These two lines are only shown for general orientation (see text). Errors are 1σ.

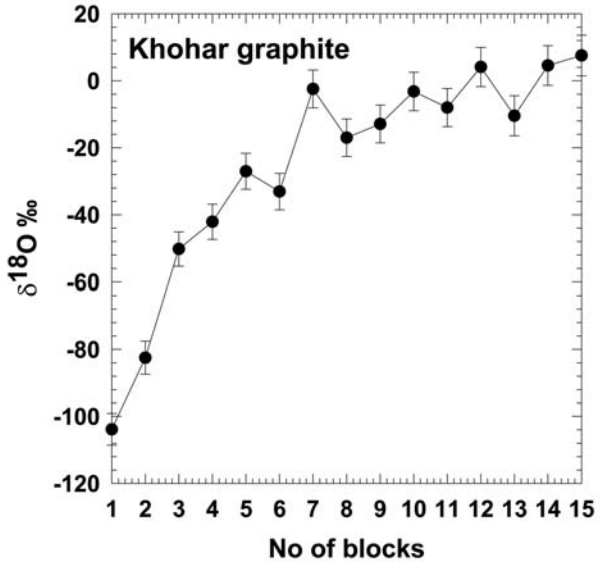

Fig. 9. Variation of $\delta^{18}O$ with time (expressed as number of analysis blocks on the same sample spot) for a vein graphite in Khohar. Depletions in ^{18}O, with $\delta^{18}O$ values starting from –100‰, are seen in the first few blocks, suggesting the presence of isotopically anomalous material that has been sputtered away during the measurement. Errors are 1σ.

Evidence for a pre-accretionary origin comes from several petrographic observations: 1) The different proportions of the graphite assemblages MAC, TAC, SAC and OAC among the chondrites (Table 2) suggest a preferential selectivity and not in situ diffusion-controlled precipitation of graphite from dissolved carbon or decomposition from carbonaceous matter and subsequent growth. 2) The high abundance of graphite in a chondrule rim in Khohar (more than 30%, see Fig. 3) suggests that the carbon was not produced by the breakdown of carbides. Rather it apparently was accreted in its present form onto the chondrule surface before any accretion of the surrounding matrix and compaction took place. 3) Different graphite morphologies are present in some metal grains as isolated inclusions within the same grain (see Fig. 5c). This suggests that pre-existing graphite grains of different morphologies were incorporated while the metal was liquid rather than produced in situ. 4) Graphite in Grady is most abundant in a specific region of the section that probably represents a portion of a clast. This indicates that the carbon in the clast is original and not a transformation product of parent body processing, which would be expected to lead to a uniform distribution of the graphite throughout the whole chondrite. It is remarkable that the most graphite-rich chondrites Khohar, Mezö-Madaras, and Grady are brecciated (Table 1). While this cannot be generalized because confirmation needs investigation of many more samples, it also argues against parent body processes being responsible for graphite formation.

Evidence for a pre-accretionary origin of the graphite is provided not only by petrographic observations, but also by the isotopic compositions. The C, N, and H isotopic heterogeneities in graphite (see discussion below) clearly suggest different sources of the carbon, which would mean that it cannot be produced during metamorphism. The association of the graphites with their host phases in the various assemblages can either have a genetic origin (i.e., both formed together under the same local conditions) or a mechanical origin (i.e., via accretion). We thus argue that the graphites are formed in the solar nebula and inherited their isotopic records from different carbonaceous precursors. This does not completely exclude the possibility of formation of some graphites during metamorphism, as certain types are preferably attributed to an origin by parent body metamorphism (Mostefaoui et al. 2000). However, we consider the role of parent body metamorphism for the production of graphite to be rather limited.

How Did the Various Graphite Morphologies Form?

It has been conjectured that the graphite morphologies are due to the diverse nature of the carbon precursors and/or due to varying conditions during graphitization (Mostefaoui et al. 2000). Because graphitization is an irreversible process (i.e., there is no chemical reaction that can trace the path back to the original carbonaceous precursors), there is no direct method to determine the nature of the precursors of the graphite with different morphologies. A possible method to

solve this problem would be to structurally characterize these morphologies and reproduce them experimentally. Below, we will present a clear descriptive scheme of the various graphite morphologies in connection with graphitization and growth mechanisms. Further, we will discuss whether remains of carbonaceous precursor materials are still present within the now observed graphite.

A Descriptive Scheme

First, it should be noted that the term morphology used here refers mainly to the external structure, which is based purely on optical microscopic observations, and not to the internal atomic structure which needs more appropriate techniques for its determination. At present, there exists no experimental study of the production of the graphite morphologies in association with meteorites except for cliftonite. Cliftonite has been known for a long time to be present in Canyon Diablo, Odessa, and in other meteorites (Brett and Higgins 1967; El Goresy 1965), and it has been experimentally produced by the breakdown of cohenite (Brett and Higgins 1967). Other morphologies, although described in the literature, have not been studied in great detail with respect to their growth mechanisms and their various crystal orientations in reflected light microscopy.

In an attempt to better characterize some of the morphologies identified in the present study, we schematically describe them on the basis of previous literature studies and on our own optical microscopy experience with respect to graphite in meteorites. Figure 10 shows projections of three-dimensional hand drawn views of single graphite fibers, spherulitic graphite, feathery graphite, graphite books, and cliftonite, as well as some of their two dimensional planes as seen in polished sections by reflected polarized light microscopy. The fibers are needles of rombohedral graphite crystals with the needle axis being along the C-axis (Ramdohr 1973). When polished and observed in reflected polarized light, the different gray levels are due to twin lamellae parallel to the C-axis (see Fig. 5b). Another arrangement of the needles, their growth from a common center, results in spherulitic graphite. Because of its symmetry, this type does not show significant changes in shape when cut along different planes (e.g., planes a and b in Fig. 10). A spectacular, even though the least common, appearance of spherulitic graphite is obtained when the plane of the cut passes exactly through the center of the sphere (plane b in Fig. 10). The spherulitic grain in Mezö-Madaras troilite (Fig. 5e) shows a good example of such a cut. Feathery graphites (Fig. 5c) are crystals grown in the shape of a fan from one or more starting points (Fig. 10). The first observed example of this type was a grain of 160 μm in diameter in Acapulco (El Goresy et al. 1995). Graphite books and cliftonite are composed of well cleaved graphite sheets. The books are single crystals having parallel layer-structured sheets with well developed cleavage along the (0001) basal plane. Depending on the plane of cut, different two-dimensional shapes can be seen (Fig. 10). Cliftonite is a polycrystalline aggregate with a cubic morphology (El Goresy 1965). It is an arrangement of single crystals of books with basal planes of increasing size from the center of the cube. Depending on the exposed polished plane, cliftonite appears as squares, rectangles, triangles, or hexagons (Fig. 10). An illustrative example of the (0100) square plane of cliftonite is a Canyon Diablo graphite grain described by Mostefaoui (1996).

Nucleation and Growth

The descriptive scheme above indicates that the graphite morphologies depend essentially on two factors: 1) the shape of the graphite sheets and 2) the stacking order of these sheets. In order to determine how graphite of different morphologies in chondrites formed, it is essential to understand the mechanisms, such as nucleation and growth, which controlled these two factors. Nucleation and growth of graphite sheets are well documented in literature. In terrestrial samples, a large variety of natural graphite forms has been studied (Kvasnitsa and Yatsenko 1999; Palache 1941; Veselovsky 1936). In anorthosite from the Ukraine, Kvasnitsa and Yatsenko (1999) found a series of graphite crystal morphologies including tabular, columnar, pseudodipyramidal, pseudodipyramidal-prismatic, and nearly spherical shapes. These morphologies are attributed to nucleation and growth along the [0001] direction in the presence of negative wedge disclinations (a class of crystal defects promoting growth forms). Crystal growth along the [0001] direction is common in graphite and can be understood from the structure of the carbon atoms in which the basal c-faces of the graphite sheets are weakly bonded to each other, resulting in the lowest energy surfaces. This allows fastest growth at the sheet edges (Freise 1962). A well-known growth pattern of the graphite in this manner is the spiral growth (known as screw dislocation, Weiner and Hager 1987), which results from defects in the crystal structure on the basal planes of graphite sheets. In chondrites, the stacking along the c-axis of the graphite books and cliftonite suggests that they could have been produced by a similar mechanism. The spherulitic morphologies are arrangements of graphite needles, and hence a different mechanism was probably responsible for their growth.

Graphite Precursors

Graphites in unequilibrated chondrites are highly disordered (see Mostefaoui et al. 2000). Because different carbonaceous precursors are expected to behave differently during the graphitization process, it is essential to understand the role of the nature of the precursors in controlling the final morphologies of the graphite. Synthesis experiments show that graphitization is a multi-step process that starts with the purification of the precursor carbonaceous matter by the loss

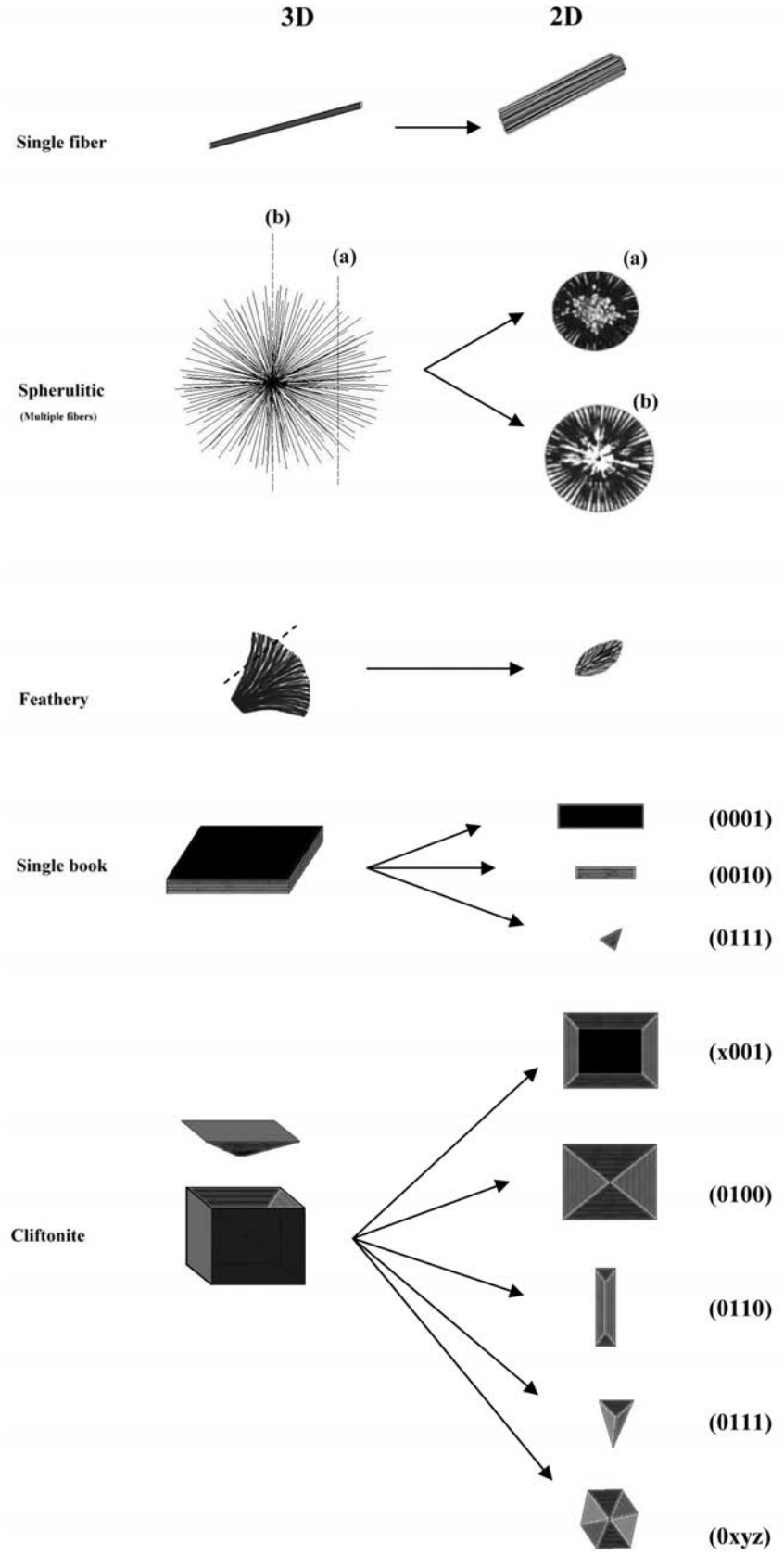

Fig. 10. Hand-drawn schematic three-dimensional (3D) projection and two-dimensional (2D) (as seen in polished thin sections by reflected polarized light optical microscopy) views of several graphite morphologies in chondrites.

of heteroatoms such as H, N, and O. This step is necessary for the development of the planar stacking layers that finally leads to the formation of ordered graphite. This shows that, whatever the nature of the precursor material, the product preceding the final ordering step must be almost pure carbon. Because our chondritic graphites are highly disordered and generally contain high concentrations of N (Table A1, see also Mostefaoui et al. 2000), they probably did not reach this level of purification. The causes of this incomplete purification process can be unpropitious conditions (e.g., low temperature, relatively oxidizing conditions) and/or an inhibiting property of the carbonaceous precursors (e.g., "nongraphitizable" carbon, see Franklin 1951). In either case, the disorder and high trace element content hints at the possibility that remains of the carbonaceous precursors have survived the graphitization process. These remains could have been a mixture of carboacaeous materials from different sources that are still present in the graphite. The chacterization of organic molecules within the graphite by appropriate techniques would be of great help in determining the nature of the precursors of the graphite in chondrites.

The Isotopic Approach

The presence of different carbonaceous precursors has probably played a significant role not only in producing the diversity of graphite morphologies but also in producing the large variations of the carbon and nitrogen isotopic compositions of the graphite in chondrites. The absence of a correlation between graphite morphologies and isotopic compositions shows that the graphitization process, temperature of formation, cooling rates in the source region, and the nature of the graphite precursors were factors that all played a role in producing the final composition of the graphite. The distinct carbon isotopic compositions of the granular graphite in Grady and, to a lesser extent, the book graphites in St. Marks, may be due to single precursors for these morphologies that did not mix with one another as for those contributing to other morphologies.

Remarkably, in the allegedly paired chondrites of "the Acfer clan," the average $\delta^{13}C$ value in Acfer 182 is significantly higher than those in Acfer 207 and Acfer 214 (Fig. 6). Paired meteorites should contain the same graphite morphologies and identical isotopic compositions (i.e., the same distribution of mixed precursors). In the Acfer meteorites, neither the C isotopic compositions nor the proportions of the phases associated with the graphite are the same (see also Table 2). This makes the pairing assignment for these chondrites questionable.

Are Any Interstellar Conditions Recorded in Chondritic Graphites?

The observed $\delta^{15}N$ values in the graphite from Khohar, Mezö-Madaras, and in Acfer 182 (and possibly also Acfer 207) range up to levels that cannot be explained by common fractionation processes occurring within the solar system. The N anomaly is probably of the same origin as those found in other meteorites, including Mezö-Madaras, Dimmitt, Y74191, Pecora Escarpment 91467, Bencubbinites, and in IDPs. For these, the anomaly was attributed to an interstellar origin. Four processes in different astrophysical environments have been proposed as possible sources of the ^{15}N enrichments: chemical fractionation in interstellar molecular clouds (IMC), explosive H burning nucleosynthesis in novae, explosive and neutrino-induced nucleosynthesis in type II supernovae (SN), and explosive He burning in type Ia SN. The enrichments in D and the lack of C isotopic anomalies favor ion-molecule reactions at low temperature in IMCs as the cause of the ^{15}N enrichments (Messenger and Walker 1996; Mostefaoui et al. 1998; 2002). While vein graphites in Khohar and Mezö-Madaras are enriched in ^{15}N and D, their oxygen isotopic ratios are normal (see Fig. 8). This is not unexpected, since O isotopic fractionation by ion-molecule reactions in IMCs is predicted to be relatively small (Langer et al. 1984). Recent calculations of ion-molecule reactions predict a maximum ^{15}N excess d in dense molecular gases of 800‰, which is lower than some of the reported results in meteorites (Charnley and Rodgers 2002; Terzieva and Herbst 2000). This seems to be inconsistent with the IMCs origin of the ^{15}N enrichments in meteorites. Because there are only few calculations of N isotopic chemistry in IMCs, which in addition are not free of uncertainties, it is difficult to arrive at a conclusive answer. Alternatively, recent theoretical work suggests that under certain circumstances ^{15}N enrichment can be produced in the solar nebula, either by molecular depletion from the gas phase onto surfaces of dust grains at 10K in the outer regions of the protosolar disk or by self-shielding in the inner part of the nebula (Charnley and Rodgers 2002; Clayton 2002). Here too, while the first mechanism suffers from the same difficulties as the IMCs hypothesis, the second is untenable because the expected large O and C isotopic anomalies are not seen in our samples.

The negative correlation of $\delta^{15}N$ with $\delta^{13}C$ in Khohar, Mezö-Madaras, and Acfer 207 graphites (see Fig. 6) suggests mixing between isotopicaly distinct reservoirs. If the ^{15}N enrichments in graphite are of an interstellar origin, then the correlation implies mixing between exotic interstellar components and solar system carbon, although terrestrial contamination cannot be totally excluded. In such a case, the exotic components (enriched in ^{15}N and depleted in ^{13}C) could have been mixed either as discrete grains or as a compound containing exotic C and N.

To What Extent do the Isotopic Compositions of Chondritic Graphites Reflect Solar Nebula Conditions?

Graphite is a highly retentive mineral for pristine H, N, and C isotopic signatures. This is seen from the preserved isotopic signatures in graphite from meteorites that experienced high temperature conditions such as Acapulco

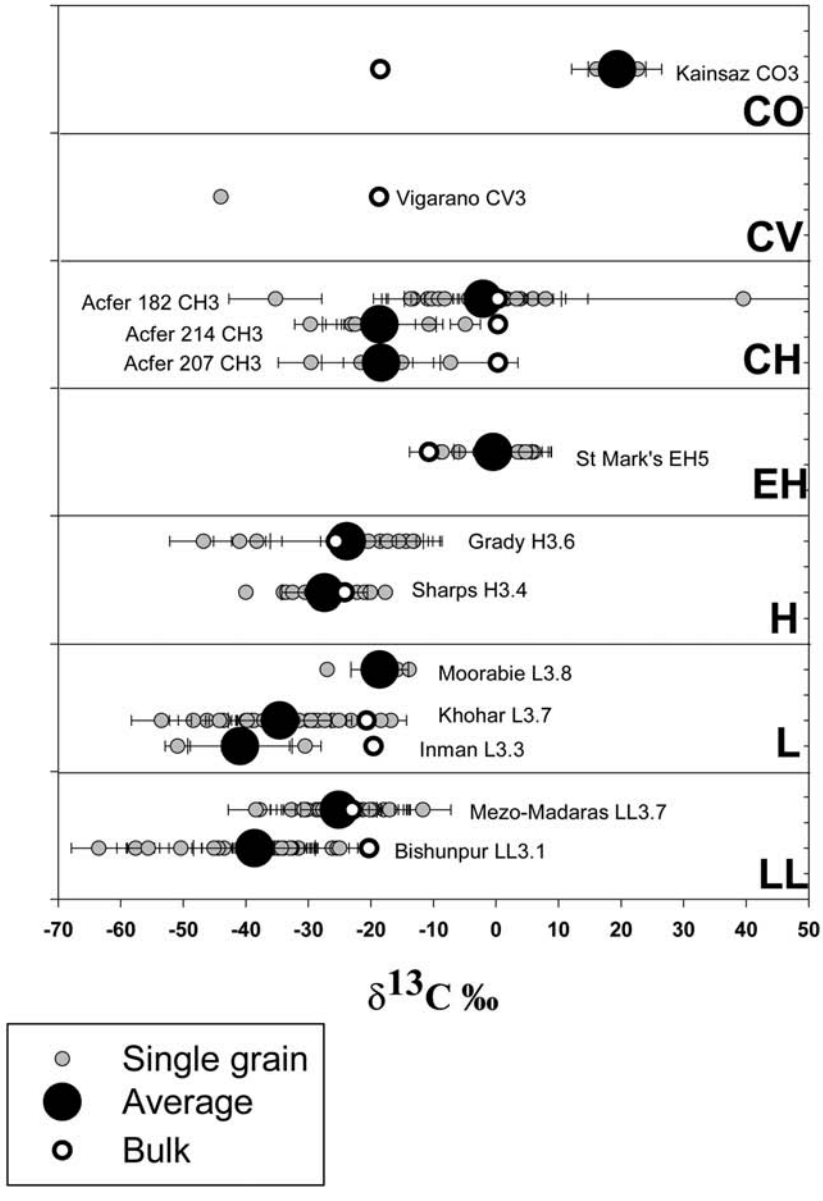

Fig. 11. Plots of the distribution of $\delta^{13}C$ values for graphite in ordinary, carbonaceous, and enstatite chondrites. The meteorite types are ordered according to decreasing oxidation state within a given class. Also plotted are the bulk $\delta^{13}C$ values of the chondrites for comparison. The data are from the present study and from Grady et al. (1982, 1986, 1989, 1991), Kerridge (1985), Perron and Fieni (2000) and Alexander et al. (1998). Errors are 1σ.

(El Goresy et al. 1995; Zipfel et al. 1995). It is also seen in the lodranite Graves Nunataks 95209 where studies suggest the presence of trapped exotic carbon remnants that did not equilibrate with each other isotopically during the extensive parent body differentiation (Nittler and McCoy 2000; Stroud et al. 2001). Unequilibrated chondrites experienced much lower temperatures than Acapulco and Graves Nunataks 95209, and morphological and isotopic data show that the graphite in chondrites has a pre-accretionary origin (see discussion above). Chondritic graphite is thus expected to preserve a record of solar nebula conditions.

In Fig. 11 we plot the carbon isotopic ratios of the graphite in ordinary, carbonaceous, and enstatite chondrites in comparison with the bulk carbon isotopic compositions of the same meteorites. The data are from the present and previous studies. A remarkable feature in Fig. 11 is that many of the chondrites have bulk $\delta^{13}C$ values that do not match the graphite $\delta^{13}C$ values. More than half of the chondrites have bulk $\delta^{13}C$ values larger than the graphite average values and only two (Kainsaz and St. Marks) have bulk $\delta^{13}C$ values smaller than the graphite averages. This means that the graphite must have a carbonaceous counterpart with isotopic signatures distinct from that of the graphite. This is consistent with our estimate of the relative

graphite abundance in chondrites which is markedly different from the relative bulk carbon abundance from stepped combustion experiments (Table 1). The previous and present studies show that, despite its common presence and wide distribution in chondrites, the graphite represents no more than one percent of the total carbon (e.g., Mostefaoui et al. 2000). The assumption that most of the step-combusted carbon in St. Marks is from graphite (Grady et al. 1986) is probably incorrect, because it is very difficult to reconcile with the fact that the bulk $\delta^{13}C$ ratio of the chondrite is clearly lower than the average graphite ratio (Fig. 11). Grady et al. (1986) did not totally exclude the possibility that cohenite ($[Fe, Ni]_3C$), which is present in enstatite chondrites and which combusts within the temperature range of graphite, could also have contributed to the total carbon budget in St. Marks. Other phases in chondrites such as metal and chondrule silicates should not be excluded as well, since significant amounts of carbon can be dissolved in them (Mostefaoui et al. 1995; Hanon et al. 1998). Stepped combustion experiments do not show large variations of $\delta^{13}C$ as function of the release temperature (Grady et al. 1989). This indicates that the abundant carbonaceous counterpart has a restricted range of carbon isotopic compositions in chondrites. This is what is expected if these carbonaceous phases are less retentive than graphite.

The question now is what isotopic signatures are expressed by the graphite. The question can be treated by referring to Fig. 11. The diagram shows two remarkable features. (i) There are significant variations in the C isotopic ratios of graphites within a given chondrite, with an apparent decreasing range of isotopic ratios with increasing petrologic types. (ii) Despite the scatter in the average graphite $\delta^{13}C$ values among different chondrites, there is a hint of a systematic increase of the mean isotopic ratio from ordinary, to enstatite, to carbonaceous chondrites (except for Vigarano CV3). This can be interpreted as being due to temporal or spatial variations of the C isotopic compositions in the regions where the graphites formed. If this is true, it implies a C isotopic heterogeneity both on a small scale (i.e., in meteorites of the same petrologic type) and on a larger scale (i.e., in meteorites from different chondrite classes) within the early solar nebula. This further indicates that the C isotopic composition of graphite reflects solar nebular conditions. This requires that graphite existed as a stable phase under the solar nebular physical conditions such as temperature and pressure and that graphite accreted at very low temperature in order to escape oxidation (Mendybaev et al. 1997). The negative trends for Khohar and Mezö-Madaras (see Fig .6) can be explained by a higher abundance of exotic N (^{15}N-enriched) in regions where C isotopic ratios were smaller (i.e., where $\delta^{13}C$ values were more negative).

CONCLUSION

A detailed survey of chondrites by reflected light microscopy revealed the presence of appreciable amounts of graphite in many of the unequilibrated members. In Khohar (L3), the graphite is much more abundant than in any other chondrite studied so far. Graphite is found in three different lithologies: in chondrules, chondrule rims, and in the matrix. Different graphite morphologies were encountered, including veins, fibers, books, spherules, granules, feathery, cliftonite, and a very fine-grained, structurally unknown, type. The presence of various graphite morphologies within a large variety of assemblages in chondrites indicates a high complexity and variability of C precursor materials and of the physico-chemical conditions under which graphite formed. The graphite morphologies are attributed to a combination of factors such as graphitization process, temperature of formation, cooling rates in the source region, and the nature of the carbonaceous precursors. The petrographic settings of the graphites are consistent with a pre-accretionnary origin of the carbon. This is supported by variations in the C, H, N isotopic compositions of the graphite. Substantial isotopic anomalies in the form of enrichments in the heavy isotopes of N and H were observed in vein and fine-grained graphites from Khohar, Mezö-Madaras and the Acfer clan chondrites. They are attributed to ion-molecule reactions at low temperatures in the interstellar molecular cloud from which the solar system formed, though they seem to be incompatible with the results of recent calculation. The C isotopic compositions of the graphite are normal (i.e., within the range of solar system ratios), but vary significantly within the same meteorite, within the same petrologic group, and among the petrographic groups. This hints at small-scale and large-scale carbon isotopic heterogeneities in the early solar system.

Acknowledgments–We are grateful to J. Janicke, V Träumer, C. Klähr, and G. Bonk for technical assistance. We thank G. Kurat, G. J. MacPherson, and F. Wlotzka for generously providing meteorite samples. The work of P. Hoppe was supported by the Swiss National Science Foundation. Reviews by N. Sugiura and an anonymous reviewer helped in improving the manuscript. The contribution of F. S. and E. Z. was supported by NASA grant NAG5-9801.

Editorial Handling—Dr. Ian Franchi

REFERENCES

Anders E. and Zinner E. 1993. Interstellar grains in primitive meteorites: Diamond, silicon carbide, and graphite. *Meteoritics* 28:490–514.

Brearley A. J. 1990. Carbon-rich aggregates in type 3 ordinary chondrites: Characterization, origin, and thermal history. *Geochimica et Cosmochimica Acta* 54:831–850.

Brearley A. J. 1999. Origin of graphitic carbon and pentlandite in matrix olivines in the Allende meteorite. *Science* 285:1380–1382.

Brett R. and Higgins G. T. 1967. Cliftonite in meteorites: A proposed origin. *Science* 156:819–820.

Charnley S. B. and Rodgers S. D. 2002. The end of interstellar

chemistry as the origin of nitrogen in comets and meteorites. *The Astrophysical Journal* 569:L133–L137.
Clayton R. N. 2002. Solar system: Self-shielding in the solar nebula. *Nature* 415:860–861.
El Goresy A. 1965. Mineralbestand und Strukturen der Graphit- und Sulfideinschlüsse in Eisenmeteoriten. *Geochimica et Cosmochimica Acta* 29:1131–1151. In German.
El Goresy A., Yabuki H., Ehlers K., Woolum D., and Pernicka E. 1988. Qingzhen and Yamato-691: A tentative alphabet for the EH chondrites. *Proceedings of the NIPR Symposium on Antarctic Meteorites* 1:65–101.
El Goresy A., Zinner E., and Marti K. 1995. Survival of isotopically heterogeneous graphite in a differentiated meteorite. *Nature* 373: 496–499.
Franklin R. E. 1951. The structure of graphitic carbons. *Acta Crystallographica* 4:253–261.
Freise E. J. 1962. Structure of graphite. *Nature* 193:671–672.
Grady M. M., Swart P. K., and Pillinger C. T. 1982. Carbon isotopic composition of some type 3 ordinary chondrites (abstract). 13th Lunar and Planetary Science Conference. pp. 277–278.
Grady M. M., Wright I. P., Carr L. P., and Pillinger C. T. 1986. Compositional differences in enstatite chondrites based on carbon and nitrogen stable isotope measurements. *Geochimica et Cosmochimica Acta* 50:2799–2813.
Grady M. M., Wright, I. P., and Pillinger C. T. 1989. A preliminary investigation into the nature of carbonaceous material in ordinary chondrites. *Meteoritics* 24:147–154.
Grady M. M., Ash R. D., Morse A. D., and Pillinger C. T. 1991. Acfer 182: An unusual chondrite with affinities to ALH 85085. *Meteoritics* 26:339–340.
Grady M. M. and Pillinger C. T. 1993. Acfer 182: Search for the location of ^{15}N-enriched nitrogen in an unusual chondrite. *Earth and Planetary Science Letters* 116:165–180.
Hanon P., Robert F., and Chaussidon M. 1998. High carbon concentrations in meteoritic chondrules: A record of metal-silicate differentiation. *Geochimica et Cosmochimica Acta* 62: 903–913.
Hashizume K., Chaussidon M., Marty B., and Robert F. 2000. Solar wind record on the Moon: Deciphering presolar from planetary nitrogen. *Science* 290:1142–1145.
Huss G. R. and Lewis R. S. 1995. Presolar diamond, SiC, and graphite in primitive chondrites: Abundances as a function of meteorite class and petrologic type. *Geochimica et Cosmochimica Acta* 59: 115–160.
Huss G. R., Hutcheon I. D., and Wasserburg G. J. 1997. Isotopic systematics of presolar silicon carbides from the Orgueil (CI) chondrite: Implications for solar system formation and stellar nucleosynthesis. *Geochimica et Cosmochimica Acta* 61:5117–5148.
Hoppe P., Amari S., Zinner E., and Lewis R. S. 1995. Isotopic compositions of C, N, O, Mg, and Si, trace element abundances, and morphologies of single circumstellar graphite grains in four density fractions from the Murchison meteorite. *Geochimica et Cosmochimica Acta* 59:4029–4056.
Kerridge J. F. 1985. Carbon, hydrogen, and nitrogen in carbonaceous chondrites: Abundances and isotopic compositions in bulk samples. *Geochimica et Cosmochimica Acta* 49:1707–1714.
Kurat G. 1970. Zur Genese des kohligen Materials im Meteoriten von Tieschitz. *Earth and Planetary Science Letters* 7:317–324. In German.
Kvasnitsa V. N. and Yatsenko V. G. 1999. Disclinations in unusual graphite crystals from anorthosites of Ukraine. *The Canadian Mineralogist* 37:951–960.
Langer W. D., Graedel T. E., Frerking M. A., and Armentrout P. B. 1984. Carbon and oxygen isotope fractionation in dense molecular clouds. *Astrophysical Journal* 277:581–604.
McKeegan K. D., Walker R. M., and Zinner E. 1995. Ion microprobe isotopic measurements of individual interplanetary dust particles. *Geochimica et Cosmochimica Acta* 49:1971–1987.
Mendybaev R. A., Beckett J. R., Grossman L., and Stolper E. 1997. Volatilization of graphite in reducing gases—Preliminary results (abstract). 23rd Lunary and Planetary Science Conference. pp. 865–866.
Messenger S. and Walker R. M. 1996. Evidence for molecular cloud material in meteorites and interplanetary dust. In *Astrophysical implications of the laboratory study of presolar materials,* edited by Bernatowicz T. J. and Zinner E. Woodbury, New York: American Institute of Physics. pp. 545–564.
Morse A. D., Wright I. P., and Pillinger C. T. 1989. Hydrogen in the Inman ordinary chondrite. 52nd Annual Meeting of the Meteoritical Society. LPI Contribution #712. p. 166.
Mostefaoui S., Perron C., Cahssidon M., Hanon P., and Robert F. 1995. Carbon in metal of primitive ordinary chondrites (abstract). *Meteoritics* 30:553–554.
Mostefaoui S. 1996. Metal et carbone dans les chondrites ordinaires primitives: Implications pour la physico-chimie du systéme solaire ancien. Ph.D. thesis, Muséum National d'Histoire Naturelle, Paris, France. In French.
Mostefaoui S., Hoppe P., and El Goresy A. 1998. In situ discovery of graphite with interstellar isotopic signatures in a chondrule-free clast in an L3 chondrite. *Science* 280:1418–1420.
Mostefaoui S., Perron C., Zinner E., and Sagon G. 2000. Metal-associated carbon in primitive chondrites: Structure, isotopic composition, and origin. *Geochimica et Cosmochimica Acta* 64: 1945–1964.
Mostefaoui S., El Goresy A., Hoppe P., Gillet P., and Ott U. 2002. Mode of occurence, textural settings and nitrogen-isotopic compositions of in situ diamonds and other carbon phases in the Bencubbin meteorite. *Earth and Planetary Science Letters* 204: 89–100.
Nittler L. R. and McCoy T. J. 2000. Carbon isotopes in graphite from lodranite Graves Nunataks 95209 (abstract). *Meteoritics & Planetary Science* 35:A120.
Alexander C. M. O'D., Russell S. S., Arden J. W., Ash R. D., Grady M. M., and Pillinger C. T. 1998. The origin of chondritic macromolecular organic matter: A carbon and nitrogen isotope study. *Meteoritics & Planetary Science* 33:603–622.
Palache C. 1941. Contributions to the mineralogy of Sterling Hill, New Jersey: Morphology of graphite, arsenopyrite, pyrite, and arsenic. *American Mineralogist* 26:709–717.
Perron C. and Fieni C. 2000. Isotopic heterogeneity of carbon and nitrogen in unequilibrated chondrites (abstract #1497). 31st Lunar and Planetary Science Conference CD-ROM.
Ramdohr P. 1973. *The opaque minerals in stony meteorites.* Amsterdam: Elsevier Publishing Company. 244 p.
Romig A. D. and Goldstein J. I. 1978. Determination of the Fe-rich portion of the Fe-Ni-C phase diagram. *Metallurgical and Materials Transactions* 9A:1599–1609.
Stroud R. M., Nittler L. R., and McCoy T. J. 2001. Microstructure of graphite with unusual carbon isotopes in lodranite Graves Nunataks 95209 (abstract). *Meteoritics & Planetary Science* 36: A200.
Sugiura N. and Kiyota K. 1998. H, C, and N isotopic compositions of graphite in three primitive ordinary chondrites (abstract #1341). 29th Lunar and Planetary Science Conference. CD-ROM.
Sugiura N. and Zashu S. 2001. Carbon-silicate aggregates in the CH chondrite Pecora Escarpment 91467: A carrier of heavy nitrogen of interstellar origin. *Meteoritics & Planetary Science* 36:515–524.

Terzieva R. and Herbst E. 2000. The possibility of nitrogen isotopic fractionation in interstellar clouds. *Monthly Notices of the Royal Astronomical Society* 317:563–568.

Veselovsky V. S. 1936. Carbon: Diamond, graphites, and coals, and methodology of their investigation. Moscow, Russia: ONTI. In Russian.

Weiner K.-L. and Hager H. 1987. Growth spirals on graphite crystals. *Lapis* 12:31–33.

Zinner E., Tang M., and Anders E. 1989. Interstellar SiC in the Murchison and Murray meteorites: Isotopic composition of Ne, Xe, Si, C, and N. *Geochimica et Cosmochimica Acta* 53:3273–3290.

Zipfel J., Palme H., Kennedy A. K., and Hutcheon I. D. 1995. Chemical composition and origin of the Acapulco meteorite. *Geochimica et Cosmochimica Acta* 59:3607–3627.

APPENDIX

Table A1. Carbon and nitrogen isotopic compositions of graphite in chondrites. In the first column, the first digit indicates the sample number, the letter(s) + corresponding digit indicate the location, and the last 1 or 2 digits indicate the measurement number. Errors are 1σ. The N concentrations were calculated using the sensitivity factor given by Hoppe et al. (1995). Concentrations up to 20000 ppm are considered accurate within a factor of 2–3. Higher concentrations are probably overestimated (Huss et al. 1997).

Sample	Run #	Location	Morphology	$\delta^{13}C$ (‰)	$\delta^{15}N$ (‰)	N (ppm)
Khohar						
1A1-1	1	SAC	Fb-B	–26 ± 2	80 ± 37	126
1A2-1	1	MAC	B	–32 ± 2	18 ± 23	694
1D1-1	1	MAC	Fb-B	–17 ± 2	36 ± 28	610
1E1-1	1	MAC	Fb-B	–23 ± 2	39 ± 17	586
2F1-1	1	MAC	V-B	–24 ± 3	76 ± 65	304
2G1-1	1	MAC	V	–36 ± 3	159 ± 101	87
2H1-1	1	MAC	V-B	–31 ± 4	12 ± 63	249
2H1-2	1	MAC	V-B	–28 ± 4	134 ± 65	284
2H1-3	1	MAC	V-B	–24 ± 4	56 ± 109	120
2H2-1	1	MAC	B	–14 ± 8	40 ± 77	1124
1AA5-1	1	SAC	Fb-B	–29 ± 3	28 ± 36	470
1AC7-1	1	MAC	V-B	–30 ± 3	25 ± 28	698
1AC7-2	1	MAC	V	–32 ± 3	302 ± 46	547
1AR1-1	1	MAC	V	–40 ± 3	522 ± 59	324
1AR1-2	1	MAC	V	–39 ± 2	583 ± 94	262
1AR1-3	1	MAC	V	–46 ± 5	384 ± 64	743
1AR1-4	1	MAC	V	–40 ± 4	654 ± 73	196
1AR1-6	1	MAC	V	–39 ± 3	955 ± 76	175
1AR1-7	1	MAC	V	–40 ± 3	825 ± 70	170
1AR1-8	1	MAC	V	–44 ± 3	938 ± 80	318
1AR1-9	1	MAC	V	–48 ± 4	694 ± 57	759
1AR1-10	1	MAC	V	–44 ± 2	733 ± 54	220
1AR1-11	1	MAC	V	–53 ± 5	817 ± 96	467
1Z1-1	1	MAC	V-B	–31 ± 5	852 ± 159	128
1Z1-2	1	MAC	V-B	–32 ± 3	764 ± 205	183
1Z1-3	1	MAC	V-B	–34 ± 3	816 ± 88	133
1Z1-5	1	MAC	V-B	–28 ± 5	507 ± 84	133
Mezö-Madaras						
A1-1	1	MAC	V	–23 ± 8	64 ± 102	864
A1-1	2	MAC	V	–23 ± 8	60 ± 104	638
A1-2	1	MAC	V	–23 ± 4	272 ± 51	641
A1-2	2	MAC	V	–30 ± 6	258 ± 65	637
A1-3	1	MAC	V	–21 ± 5	159 ± 43	1258
A1-3	2	MAC	V	–24 ± 3	276 ± 45	745
A1-4	1	MAC	V	–27 ± 4	126 ± 46	866
A1-5	1	MAC	V	–26 ± 4	224 ± 41	801
A1-6	1	MAC	V	–28 ± 4	202 ± 44	899
A2-1	1	SAC	Fb-B	–22 ± 8	55 ± 178	216
B1-1	1	MAC	V	–24 ± 4	188 ± 46	953

Table A1. *Continued.* Carbon and nitrogen isotopic compositions of graphite in chondrites. In the first column, the first digit indicates the sample number, the letter(s) + corresponding digit indicate the location, and the last 1 or 2 digits indicate the measurement number. Errors are 1σ. The N concentrations were calculated using the sensitivity factor given by Hoppe et al. (1995). Concentrations up to 20000 ppm are considered accurate within a factor of 2–3. Higher concentrations are probably overestimated (Huss et al. 1997).

Sample	Run #	Location	Morphology	$\delta^{13}C$ (‰)	$\delta^{15}N$ (‰)	N (ppm)
B1-1	2	MAC	V	–18 ± 4	92 ± 38	850
B1-2	1	MAC	V	–26 ± 6	267 ± 64	815
B1-2	2	MAC	V	–20 ± 4	145 ± 39	728
G1-1	1	MAC	V-B	–28 ± 5	171 ± 27	1453
G1-2	1	MAC	V	–22 ± 4	191 ± 29	1427
G1-5	1	MAC	B	–26 ± 4	64 ± 22	2222
B5-1	1	MAC	B	–37 ± 8	–31 ± 14	<36,771
C1-1	1	TAC	S	–33 ± 3	147 ± 56	262
F1-1	1	MAC	Fb-B	–22 ± 3	–30 ± 42	331
F1-2	2	MAC	Fb-B	–20 ± 3	45 ± 71	178
F2-1	1	MAC	Fb-B	–17 ± 3	32 ± 46	396
E1-1	1	SAC	Fb-B	–12 ± 4	39 ± 65	449
B1-3	1	MAC	V	–31 ± 4	225 ± 44	593
Inman						
A1-1	1	OAC	G	–41 ± 3	-19 ± 27	2464
A1-2	1	OAC	G	–30 ± 2	2 ± 21	1113
B1-1	1	MAC	C	–51 ± 2	14 ± 26	389
C1-1	1	MAC	Fg-B	–41 ± 2	91 ± 40	473
Acfer 207						
B1-1	1	SAC	B	–15 ± 5	89 ± 69	578
C1-1	1	SAC	Fg-B	–7 ± 11	15 ± 79	1427
D1-1	1	SAC	Fg-B	–22 ± 8	99 ± 42	2210
D1-2	1	SAC	Fg-B	–30 ± 5	167 ± 28	1032
Acfer 214						
A1-1	1	SAC	Fg-B	–21 ± 3	65 ± 18	1371
A1-2	1	SAC	Fg-B	–30 ± 2	140 ± 31	1440
A1-3	1	SAC	Fg-B	–23 ± 2	65 ± 14	2522
A1-4	1	SAC	Fg-B	–22 ± 2	30 ± 20	682
B1-1	1	MAC	Fg-B	–5 ± 2	32 ± 48	231
D1-1	1	SAC	Fg-B	–11 ± 2	42 ± 18	1027
Acfer 182						
A-a.1	1	MAC	B	1 ± 3	–23 ± 13	812
A-b.1	1	MAC	B	–1 ± 3	162 ± 25	610
A-c.1	1	MAC	B	–2 ± 4	60 ± 14	5208
A-d.1	1	MAC	B	2 ± 3	137 ± 18	1085
A-e.1	1	MAC	B	1 ± 3	149 ± 27	714
B-a.1	1	SAC	Fg-B	–4 ± 4	75 ± 14	2464
B-b.1	1	SAC	Fg-B	–4 ± 3	218 ± 23	664
B-c.1	1	SAC	Fg-B	–11 ± 9	49 ± 12	<63,560
B-d.1	1	SAC	Fg-B	–13 ± 4	351 ± 28	868
C-a.1	1	SAC	B	1 ± 3	41 ± 10	2940
C-b.1	1	SAC	B	6 ± 3	58 ± 14	966
C-c.1	1	SAC	B	4 ± 3	44 ± 15	1232
C-d.1	1	SAC	B	0 ± 3	54 ± 11	938
C-e.1	1	SAC	B	8 ± 3	145 ± 23	331
D-a.1	1	SAC	B	1 ± 3	231 ± 19	1141
D-b.1	1	SAC	B	–4 ± 4	87 ±13	2947
E1-a.1	1	SAC	Fg-B	–14 ± 5	61 ± 14	18,620
E1-b.1	1	SAC	Fg-B	–10 ± 3	211 ± 15	1778
E1-c.1	1	SAC	Fg-B	–9 ± 3	321 ± 12	2030
E1-d.1	1	SAC	Fg-B	–35 ± 7	–13 ± 8	<88,900

Table A1. *Continued.* Carbon and nitrogen isotopic compositions of graphite in chondrites. In the first column, the first digit indicates the sample number, the letter(s) + corresponding digit indicate the location, and the last 1 or 2 digits indicate the measurement number. Errors are 1σ. The N concentrations were calculated using the sensitivity factor given by Hoppe et al. (1995). Concentrations up to 20000 ppm are considered accurate within a factor of 2–3. Higher concentrations are probably overestimated (Huss et al. 1997).

Sample	Run #	Location	Morphology	$\delta^{13}C$ (‰)	$\delta^{15}N$ (‰)	N (ppm)
E2-a.1	1	MAC	Fg-B	3 ± 3	276 ± 17	1064
E2-b.1	1	MAC	Fg-B	–8 ± 3	154 ± 16	756
F1.1	1	SAC	Fg-B	40 ± 34	395 ± 63	<30,380
F1.2	1	SAC	Fg-B	–1 ± 16	438 ± 30	<33,180
Grady						
B1-1	1	TAC	B	–13 ± 4	–43 ± 35	357
B1-1	2	TAC	B	–24 ± 4	–10 ± 25	553
B1-1	3	TAC	B	–18 ± 4	4 ± 15	476
B2-1	1	TAC	B	–14 ± 4	3 ± 20	588
B2-1	2	TAC	B	–13 ± 4	28 ± 22	560
C2-1	1	MAC	Fg-B	–17 ± 5	–34 ± 18	497
C3-1	1	SAC	Fg-B	–16 ± 5	4 ± 18	497
C3-1	2	SAC	Fg-B	–20 ± 4	37 ± 20	511
J4-1	1	SAC	G	–38 ± 4	1 ± 13	1372
J4-1	2	SAC	G	–47 ± 5	9 ± 10	<27,622
J4-1	3	SAC	G	–41 ± 4	15 ± 14	910
St. Marks						
A1-1	1	SAC	B	6 ± 3	–15 ± 12	672
A1-2	1	SAC	B	6 ± 3	1 ± 21	308
A2-1	1	MAC	B	–3 ± 3	15 ± 11	1246
A2-1	1	MAC	B	0 ± 3	12 ± 18	546
B1-1	1	MAC	B	–9 ± 3	–8 ± 11	1106
B1-2	1	MAC	B	–6 ± 3	–10 ± 11	1078
C1-1	1	MAC	B	–11 ± 3	5 ± 19	658
C1-2	1	MAC	B	–9 ± 3	1 ± 15	609
D1-1	1	TAC	B	1 ± 3	44 ± 37	392
D1-2	1	TAC	B	4 ± 3	–60 ± 31	308
D3-1	1	TAC	B	3 ± 3	–34 ± 21	455
D3-2	1	TAC	B	6 ± 3	13 ± 38	280
D3-3	1	TAC	B	5 ± 4	–22 ± 48	560

Table A2. Hydrogen isotopic compositions of graphite in Khohar and Mezö-Madaras. Errors are 1σ.

Sample	Run #	Location	Morphology	δD (‰)	H (ppm)	N (ppm)
Khohar						
1AR D/H-2	24	MAC	V	83 ± 32	1457	107
1AR D/H-3	25	MAC	V	32 ± 29	1469	97
1AR D/H-4	26	MAC	V	122 ± 45	1609	87
1AR D/H-5	27	MAC	V	85 ± 44	1368	108
1AR D/H-6	28	MAC	V	39 ± 52	2299	238
1AC D/H-1	29	MAC	V	37 ± 30	3100	117
1AC D/H-2	30	MAC	V	336 ± 42	2732	190
1AC D/H-3	31	MAC	V	251 ± 32	2800	319
Mezö-Madaras						
MM3_1	1		B	–242 ± 14	–	–
MM3_1	2		B	–232 ± 8	–	–
MM3_1	3		B	–256 ± 13	–	–
MM3_1	4		B	–212 ± 11	–	–
MM3_1	5		B	–234 ± 17	–	–

Table A2. *Continued.* Hydrogen isotopic compositions of graphite in Khohar and Mezö-Madaras. Errors are 1σ.

Sample	Run #	Location	Morphology	δD (‰)	H (ppm)	N (ppm)
MM3_2	2		B	–202 ± 10	–	–
MM3_2	3		B	–214 ± 15	–	–
MM3_2	4		B	–220 ± 17	–	–
MM3_2	5		B	–210 ± 6	–	–
MM3_2	6		B	–216 ± 13	–	–
MM3_3	1		B	–240 ± 22	–	–
MM3_3	2		B	–240 ± 24	–	–
MM3_3	3		B	–236 ± 14	–	–
MM3_4	1		B	–253 ± 12	–	–
MM3_4	2		B	–280 ± 14	–	–
MM3_4	3		B	–257 ± 18	–	–
MM3_4	4		B	–267 ± 16	–	–
MM3_4	5		B	–236 ± 15	–	–
MM3_5	1		V	–201 ± 21	–	–
MM3_5	2		V	–173 ± 18	–	–
MM3_6	1		V	146 ± 9	–	–
MM3_6	2		V	207 ± 18	–	–
MM3_6	3		V	241 ± 17	–	–
MM3_6	4		V	277 ± 9	–	–
MM3_6	5		V	286 ± 12	–	–
MM3_6	6		V	296 ± 10	–	–
MM3_6	7		V	318 ± 18	–	–
MM3_6	8		V	318 ± 11	–	–
MM3_6	9		V	339 ± 11	–	–
MM3_6	10		V	360 ± 15	–	–
MM3_6	11		V	320 ± 11	–	–
MM3_6	12		V	329 ± 11	–	–
MM3_6	13		V	324 ± 26	–	–
MM3_7	1		V	182 ± 9	–	–
MM3_7	2		V	155 ± 15	–	–
MM3_7	3		V	218 ± 18	–	–
MM3_7	4		V	163 ± 13	–	–
MM3_8	1		V	–268 ± 10	–	–
MM3_8	2		V	–234 ± 15	–	–
MM3_8	3		V	–155 ± 21	–	–
MM3_8	4		V	–174 ± 23	–	–
MM3_8	5		V	–156 ± 11	–	–
MM3_8	6		V	–152 ± 12	–	–
MM3_8	7		V	–170 ± 12	–	–
MM310	1		B	–277 ± 13	–	–
MM310	2		B	–277 ± 15	–	–
MM310	3		B	–270 ± 10	–	–
MM310	4		B	–236 ± 6	–	–
MM310	5		B	–236 ± 13	–	–
MM310	6		B	–226 ± 10	–	–
MM311	1		B	–241 ± 9	–	–
MM311	2		B	–262 ± 10	–	–
MM311	3		B	–248 ± 7	–	–
MM311	4		B	–237 ± 10	–	–
MM311	5		B	–245 ± 10	–	–
MM311	6		B	–249 ± 10	–	–
MM313	1		V-B	–39 ± 9	–	–
MM313	2		V-B	–49 ± 12	–	–
MM313	3		V-B	–66 ± 17	–	–
MM314	1		V-B	–251 ± 13	–	–
MM314	2		V-B	–208 ± 15	–	–
MM315	1		V-B	–265 ± 10	–	–

Table A2. *Continued.* Hydrogen isotopic compositions of graphite in Khohar and Mezö-Madaras. Errors are 1σ.

Sample	Run #	Location	Morphology	δD (‰)	H (ppm)	N (ppm)
MM315	2		V-B	–262 ± 10	–	–
MM315	3		V-B	–210 ± 14	–	–
MM315	4		V-B	–209 ± 8	–	–
MM315	5		V-B	–187 ± 7	–	–
MM315	6		V-B	–177 ± 12	–	–
MM315	7		V-B	–165 ± 9	–	–
MM315	8		V-B	–172 ± 22	–	–
MM315	9		V-B	–180 ± 10	–	–
MM317	1		V	248 ± 18	–	–
MM317	2		V	435 ± 33	–	–
MM317	3		V	430 ± 11	–	–
MM317	4		V	519 ± 14	–	–
MM317	5		V	548 ± 29	–	–
MM317	6		V	569 ± 19	–	–
MM317	7		V	541 ± 20	–	–
MM317	8		V	539 ± 26	–	–
MM317	9		V	587 ± 21	–	–

Table A3. Oxygen isotopic compositions of graphite in Khohar and Mezö-Madaras relative to that of a terrestrial graphite standard. Slope: slope of the major axis of the error ellipse. Errors are 1σ.

Sample	Location	Morphology	Run #	$\delta^{17}O$ (‰)	$\delta^{18}O$ (‰)	Slope
Khohar						
2D1-1	MAC	V-B	1	8 ± 9	–13 ± 15	0.62
2F1-1	MAC	V-B	1	–13 ± 9	–2 ± 15	0.66
2I1-1	MAC	V	1	–	0 ± 3	–
2I1-1	MAC	V	2	17 ± 9	21 ± 15	0.58
2I1-2	MAC	V	1	–	–13 ± 3	–
2I1-2	MAC	V	2	–	–14 ± 4	–
2I1-3	MAC	V	1	–	–1 ± 3	–
2I1-3	MAC	V	2	–	4 ± 3	–
2I1-4	MAC	V	1	–	0 ± 3	–
2I1-4	MAC	V	2	–	–9 ± 4	–
2M1-1	MAC	V	1	–	–25 ± 9	–
2M1-1	MAC	V	2	–	–2 ± 3	–
2M1-1	MAC	V	3	6 ± 8	24 ± 14	0.54
2M2-1	MAC	V	1	2 ± 11	2 ± 16	1.12
2M2-1	MAC	V	2	6 ± 8	–2 ± 15	0.45
2N1-1	MAC	V	1	–	–3 ± 3	–
2N1-1	MAC	V	2	–	–9 ± 3	–
Mezö-Madaras						
A1				–5 ± 8	–12 ± 14	0.54
B1				8 ± 9	–11 ± 17	0.34
B1a				0 ± 9	–6 ± 15	0.65
B3				5 ± 8	–7 ± 14	0.53
B4				0 ± 7	6 ± 14	0.47
#1				10 ± 7	11 ± 9	0.44
#2				–3 ± 8	12 ± 11	3.80
#3				7 ± 7	17 ± 9	0.55
#4				6 ± 7	12 ± 9	1.27
#5				0 ± 7	10 ± 9	0.63
#6				1 ± 7	17 ± 9	0.91
#7				5 ± 7	3 ± 9	0.47
#8				2 ± 7	6 ± 9	0.51
#9				–4 ± 7	2 ± 9	0.64
#10				–3 ± 7	0 ± 10	0.31